THE ANISOTROPIC POTENTIAL FOR NO-INERT GAS SYSTEMS

H. H. W. THUIS

THE ANISOTROPIC POTENTIAL FOR NO-INERT GAS SYSTEMS

PROMOTOR:

PROF.DR. J. REUSS

CO-REFERENT:

DR. S. STOLTE

THE ANISOTROPIC POTENTIAL FOR NO-INERT GAS SYSTEMS

PROEFSCHRIFT

TER VERKRIJGING VAN DE GRAAD VAN DOCTOR
IN DE WISKUNDE EN NATUURWETENSCHAPPEN
AAN DE KATHOLIEKE UNIVERSITEIT TE NIJMEGEN,
OP GEZAG VAN DE RECTOR MAGNIFICUS
PROF. DR P.G A B WIJDEVELD
VOLGENS BESLUIT VAN HET COLLEGE VAN DECANEN
IN HET OPENBAAR TE VERDEDIGEN
OP DONDERDAG 1 NOVEMBER 1979
DES NAMIDDAGS TE 4 UUR

DOOR

HENRICUS HERMANUS WILHELMUS THUIS

geboren te Huissen

KRIPS REPRO MEPPEL
1979

Allen die op enigerlei wijze bijgedragen hebben tot het tot stand komen van dit proefschrift wil ik bedanken. In het bijzonder wil ik vermelden:

De leden van de groep Atoom- en Molecuulfysica van de Katholieke Universiteit te Nijmegen met wie ik zo prettig heb samengewerkt.

Drs. Monique Jacobs en drs. Dick Klaassen voor hun assistentie bij het vervaardigen van de computerprogramma's.

Drs. Dirk van den Ende en Harry Schraven die tijdens hun afstudeerperioden aan het onderzoek hebben meegewerkt.

Cor Sikkens, John Holtkamp en Frans van Rijn voor hun hulp op technisch en electronisch gebied.

Leo Hendriks die in de tijdnoodfase een aantal tekeningen verzorgde.

Loes van Doorn die het typewerk en de lay out verzorgde.

De dienstverlenende afdelingen in de personen van de heren J. van Langen, P. Walraven, H. Verschoor en H. Boltze.

De afdeling fotografie in de personen van de heren J. Spruyt en G. Dekkers.

Het onderzoek is een gedeelte van het onderzoekprogramma van de 'Stichting voor Fundamenteel Onderzoek der Materie" (F.O.M.), welke financiëel gesteund wordt door de "Nederlandse Organisatie voor Zuiver Wetenschappelijk Onderzoek" (Z.W.O.).

Voor mijn ouders

Voor Trees,

Jeroen en Ingrid

C O N T E N T S

CHAPTER 1

INTRODUCTION

The study of the angle dependence of the intermolecular potential (AIP) is one of the main topics of the Atomic and Molecular Physics Group of the Nijmegen University.

This angle dependence plays an important role in all kind of processes such as rotational transitions, reorientation processes, relaxation phenomena, rotational cooling in supersonic beams for the purpose of high quality spectroscopic measurements, determination of steric factors and rotational energy dependence of chemical reactions and possibly it plays a role in interstellar inversion processes.

During the last few years several experimental methods have been developed to gather information on the AIP. For instance, the study of rainbow scattering of atoms with several poly-atomic molecules by Buck and coworkers, or the differential measurements of inelastic transitions (i.e. HD-Ne) by the same group. Another source of information concerning the AIP is the dimer spectroscopy in beams. The activity in this field is connected mainly to Klemperer and (ex)coworkers at Harvard. An extensive discussion of these and other experiments (being often complementary) is given in chapter 2.

The measurements of the total collision cross section have proved to be an excellent and direct method, too, to investigate the intermolecular potential (IP). The experiment described in chapter 3 uses this method in combination with preferential orientation of one of the colliding particles, i.e. NO-inert gases, where NO is the molecule to be

oriented. We have to perform state selection for the NO-molecule in order to pick out a single m_j-substate to obtain the wanted preferential orientation. Once this state is selected, one can c h a n g e the preferential orientation using different directions of a B-field in the scattering region. This method is based on the early measurements of Bennewitz *et al.* and was successfully employed by Zandee, using H_2 as the molecule to be state selected. The NO-molecule can be selected rather efficiently in the $\Pi_{3/2}$ state ($j = m_j = \Omega = 3/2$) by an electric sixpole due to its nearly perfect linear Stark effect. The measurements of the anisotropy A - the relative difference of the total cross section for two different orientations of the molecule - are performed over a wide velocity range and reveal many glory extrema. This velocity dependent quantum mechanical interference pattern contains valuable information concerning the IP at distances near the position of the potential well.

Total cross section measurements without state selection (performed by J. van den Biesen, Leiden) are included in the analysis. The quenching of the glories of these data originates from the AIP.

The absolute value of the total cross section, the quenching of the isotropic glories, the position of the glories with respect to the relative velocity, the velocity averaged value of the anisotropy and its glory behaviour are the principal pieces of information gathered by us. Although complementary, these pieces are insufficient to construct the total potential for the systems studied (NO-Ne, -Ar, -Kr, -Xe). This thesis contains therefore a faint outline of the IP; some parts of the picture assume clearer features, other remain rather misty (for instance, how the AIP joins the long range tail, known from

perturbation treatments). Less vague information is obtained for the important intermolecular distances 3.5 Å < R < 10 Å.

At the moment that this work was started no satisfying theoretical description of the anisotropy A was available. Although the infinite order sudden approximation (IOS) is very useful in many fields and is put forward by several groups, it completely fails with respect to the anisotropy A. Encouraged by the H_2-results of Zandee we believed in the suitability of a linear approach (distorted wave approximation (dwa) or linear sudden approximation (lsa)) for a long time but the more experimental data became available, the more difficult it was to stick to linear theory. We developed a more involved theory, i.e. sudden approximation (sa), which is exact in first order and deals with higher order terms, in an approximate way. Nevertheless, this approximation has its own disadvantages (it is much more complicated than IOS and it employs classical trajectories obtained solely from the isotropic part of the potential).

The present investigation was started in 1968 by Stolte who built the original version of the rather complicated NO beam machine. The anisotropic glory was discovered in collaboration with H. Schwartz (1973). Molecular scattering partners were investigated by Kessener (1975).

It was a long journey from the prime results to the full body of data incorporated in the present thesis. Substantial improvements of the machine were needed to gather the information which gives us finally some feeling now the anisotropic systems NO-inert gases look alike. Still, the journey is not yet finished (as no research ever is). New problems showed up as some questions were solved underway - but at

least some questions found their proper answers (Fig. 4.3).

CHAPTER 2

THE STUDY OF ANISOTROPIC POTENTIALS BY MOLECULAR BEAMS

2.1. INTRODUCTION

The anisotropy of intermolecular potentials is subject of theoretical and experimental investigations, since many years. All rotational energy transfer processes are governed by the strength of the angle dependent part of the intermolecular potential (AIP). In addition, reorientation processes and the orientational dependence of the elastic cross section depend strongly on the AIP.

We shall limit our considerations to recent neutral molecular beam work. The theoretical aspects of anisotropy can be divided into two parts. There is the continuing effort of many quantum chemists to produce potential surfaces either by ab initio or by semi-empirical methods (refs. 1-4 and chapter 2 from ref. 5); on the other hand, one has the difficult and fastly expanding body of experience and methods leading from the potential to cross sections (see for instance chapter 3-6 of ref. 5).

The experimental part of the theme will be emphasized in the following. Energy transfer processes were recently reviewed by Faubel and Toennies (ref. 7). Consequently, experiments of 1977 and later will mainly be discussed together with those not taken into account in ref. 7, because they do not fall under the category of rotational and/or vibrational excitation experiments. Especially total collision cross section measurements with state selected beams (refs. 8-21), dimer spec-

troscopic results (refs. 22-35) and the rainbow measurements of Buck and co-workers on Na colliding with polyatomic molecules (refs 36-39) belong to the favorite objects of this comment.

The comment is subdivided according to the employed experimental techniques differential measurements without time of flight analysis (TOF) in section 2, dito with TOF analysis, however, not (fully) state resolved in section 3, dito with the single rotational state resolved in section 4, total cross section with state selection in section 5, differential and integral measurements with state selection, in nearly forward direction, in section 6, total inelastic cross section obtained using state selection and laser fluorescence in section 7, quenching of glories and other interference patterns in section 8, and dimer spectroscopy in section 9

2.2. DIFFERENTIAL COLLISION CROSS SECTION MEASUREMENTS WITHOUT TOF

In this section we mainly summarize results obtained from an analysis of the peculiar rainbow behaviour observed under condition of high energy resolution for collisions of Na with poly-atomic molecules of tetrahedral symmetry (refs. 36-39) and of K with methyliodide (ref. 40). The peculiarity consists (a) in the occurrence of a double rainbow ($Na(CH_3)_3CBr$, $-(CH_3)_3CCl$, $-(CH_3)_3CI$ and $-CH_3I$), (b) in a blurring of the rainbow accompanied by a long tail at its high angle side ($Na-C_6H_6$, $-C_{11}H_{10}$), (c) for reactive systems, in a sharp intensity drop at the high angle side of the rainbow ($Na-CCl_4$, $-GeCl_4$, $-SiCl_4$) and (d) in a strong smearing out of the primary rainbow ($Na-SnCl_4$ and $-CBr_4$). In case of reactive systems, the interpretation is based upon a combi-

nation of an optical potential and the AIP which is treated in sudden approximation. Results are collected in Table 2.1 (ref. 39). The poten-

System	ε [meV]	R_m [Å]	a_1	a_2	a_3	$\tilde{a}_3 - 0.4\,\tilde{b}_3$	$Q_{\perp}$ [Å^2]	Ref.
$(CH_3)_3CCl$-Na	22.7 ± 0.7	5.57 ± 0.3	0.3	0.15			38	36
$(CH_3)_3CBr$-Na	26.0 ± 0.8	5.61 ± 0.3	0.3	0.25	-0.05		38	36
$(CH_3)_3CI$-Na	28.1 ± 0.9	5.98 ± 0.3	0.25	0.2	-0.05		45	36
$(CH_3)_3I$-Na	27.2 ± 0.8	4.35 ± 0.3	0.2	0.05	-0.2		35	36
CH_3I-Ar *)	22.6 ± 2.0	4.00 ± 0.5	0.2	0.4				36
Na-CCl_4	21.8 ± 0.5	6.3 ± 0.2					64	38
Na-$SiCl_4$	20.4 ± 0.8	4.6 ± 0.2				0.90 ± 0.07	11	38
Na-$GeCl_4$	28.1 ± 0.9	6.5 ± 0.2					100	38
$(CH_3)_4C$-Na	18.4 ± 0.5	5.5 ± 0.2				0.20 ± 0.10		38
$(CH_3)_4Si$-Na	18.7 ± 0.8	6.3 ± 0.2				0.44 ± 0.06		38
$(CH_3)_4Sn$-Na	21.5 ± 0.8	8.3 ± 0.3				0.70 ± 0.07		38

*) $b_1 = 0.4$, $b_2 = 0.4$

Table 2.1. Anisotropy parameters from rainbow measurements. The parameters a_i and b_i are defined in Eq. (2.1), $\tilde{a}_3$ and $\tilde{b}_3$ in Eq. (2.2).

tial parameters belong to a LJ potential of the form

$$V(R,\gamma) = \left(\frac{R_m}{R}\right)^{12} \left[1 + \sum_{\lambda=1}^{3} b_\lambda P_\lambda(\cos\lambda)\right] \qquad (2.1)$$

$$- 2\varepsilon\left(\frac{R_m}{R}\right)^{6} \left[1 + a_1 \frac{R_m}{R} P_1(\cos\gamma) + a_2 P_2(\cos\gamma) + a_3 \frac{R_m}{R} P_3(\cos\gamma)\right]$$

or, if the collision partners possess tetrahedral symmetry

$$V(R,\gamma,\chi) = \varepsilon\left[\left(\frac{R_m}{R}\right)^{12} - 2\left(\frac{R_m}{R}\right)^{6}\right] \qquad (2.2)$$

$$- i\varepsilon\left[\frac{2\pi}{105}\right]^{1/2}\left[Y_{32}(\gamma,\chi) - Y_{3-2}(\gamma,\chi)\right]\left[\tilde{b}_3\left(\frac{R_m}{R}\right)^{12} - 2\tilde{a}_3\left(\frac{R_m}{R}\right)^{7}\right]$$

The accuracy of the given anisotropy parameters a_i, b_i, $\tilde{a}_3$, and $\tilde{b}_3$ is estimated to be about 10% if not indicated otherwise in Table 2.1. Depth and position of the potential minimum are given by ε and R_m. The angle γ is spanned by the intermolecular position vector and the symmetry axis of the molecule, for Eq. (2.1); in case of Eq. (2.2), the molecular axis is defined along the ζ-axis, if the tetrahedron corners are at $(\xi,\eta,\zeta) = (1,1,1)$, $(1,-1,-1)$, $(-1,1,-1)$ and $(-1,-1,1)$; χ describes a rotation around the ζ-axis.

In Table 2.1 the estimated total reactive cross section Q_R furnishes valuable information obtained from an opacity function treatment. Systems with large Q_R do not yield information on the repulsive anisotropy parameter b_1 and $\tilde{b}_3$.

2.3. DIFFERENTIAL MEASUREMENTS WITH TOF ANALYSIS OF THE SCATTERED MOLECULES; THE STATES ARE NOT (FULLY) RESOLVED

The first experiment of this type was performed by Blythe *et al.* (ref. 41) on the system $K + D_2$ followed by many other groups whose work has been reviewed by Faubel and Toennies (ref. 7). For heavy systems ($Ar-CO_2$, ref. 42, for instance) the scattering is characterized by the occurrence of many quantum jumps $\Delta j = 10-40$ indicating that the AIP

must contain Legendre polynomials with $\lambda >> 3$ (see Eq. (2.4)) and/or that the anisotropy parameters are very large so that higher order processes become very likely. Regarding the repulsive part of the interaction of this system, a theoretical investigation of Parker et al. (ref. 43) yields very strong contributions for Legendre polynomials up to $\lambda = 10$. For instance, $a_2 = q_{2,6} = 0.23$, $q_{2,8} = 0.87$, $q_{4,8} = 0.17$ describe the long range behaviour in

$$V_{LR} = - \sum_n (C_n/R^n)[1 + \sum_{\lambda>0} q_{\lambda,n} P_\lambda(\cos\theta)] \qquad (2.3)$$

and, for $R \approx R_m$, one finds in ref. 43

$$|V_0| \approx \frac{1}{10} V_2 \approx \frac{2}{30} V_4 \approx 5\ V_6 \sim 30\ V_8 > 0$$

using

$$V = \sum_\lambda V_\lambda(R) P_\lambda(\cos\theta) \qquad (2.4)$$

The experimental and theoretical results of refs. 42 and 43 both indicate that the ATP generally consists of many terms of large magnitude which all together determine the observable inelastic transition probability. Whether this situation shall force us to employ hard ellipsoids and similar models to describe nature remains to be seen; the present authors hope not. For further information the reader is referred to the review article (ref. 7) and the literature quoted therein.

This section deals with the ideal experimental situation which has come into reach only very recently (refs. 44-49). The systems under investigation at this moment are HD-Ne, HD-D_2, HD-HD, HD-He and Na_2-He and Na_2-Ne. Except for the Na_2-systems where level depletion and detection after the collision by laser fluorescence is utilized (ref. 49) the choice of the system is dictated by kinematics requiring a velocity change due to an inelastic event larger than the primary beam velocity spread and the TOF resolution. Quite naturally, molecular hydrogen appears as the ideal projectile with the drawback that its anisotropy is rather small leading to intensity problems. Buck et al. (refs. 45 and 46) reduce this difficulty by employing a random chopper TOF technique. Moreover, the authors use HD as collision partner because the inelastic collision probability is much increased due to the eccentricity of this molecule, without, however, obscuring the influence of the V_2-term (see Eq. (2.4)) which is of basic interest. The evaluation of the results in terms of a V_2-interaction is only possible because of the precise knowledge of the V_0-term. The AIP is mainly probed at $R < R_r$, by this technique.

The experimental novelty of the work of Gentry and Giese (refs. 47 and 48) consists in the introduction of a pulsed primary beam; this not only reduces the pumping requirements and leads to low background signals but also permits the use of large nozzle diameters important for the achievement of high Mach numbers (depending on pd) without being troubled by untimely production of clusters (depending on $pd^{0.55}$); here, p is the source pressure and d the nozzle diameter.

These very recent results on inelastic transition probabilities of the hydrogen molecule HD are still in the process of being evaluated. For H_2-H_2, a new, rather advanced ab initio calculation is at hand (ref. 50), whereas for H_2-Ne and H_2-He, semi-empirical potentials were discussed and compared to ab initio results recently (ref. 51). As far as the Göttingen-measurements are concerned the experimental results necessitate substantial improvements of the already rather well known potential surfaces (ref. 52).

The Kaiserslautern-measurements (ref. 49) were only just started; they look very promising and seem to indicate the path to fully state resolved differential cross sections for systems other than hydrogenic ones with their relatively large spacing of rotational levels. Here, the detection is based on laser fluorescence of Na_2-molecules scattered under a fixed laboratory angle; different rotational lines can be looked at using a cw tunable dye probe laser. To label the incoming molecules in a specific rotational state, an (on-off modulated) similar laser system is employed as pump laser upstream the scattering region. The thus modulated detector signal contains the fully state resolved information. The theoretical interpretation of these fine grained results is not yet available.

2.5. TOTAL CROSS SECTION MEASUREMENTS WITH STATE SELECTION

Older measurements of this type have been reviewed in ref. 21 so that we can confine ourselves to recent results. The method is based on the use of electrostatic (CsF, TlF, NO) or magnetic (H_2) state selectors which permit to single out and mark molecules in well defined

quantum states. For instance, a sixpole is suited to focus monochromatic NO-molecules with $j = m_j = \Omega = 3/2$ (selected state quantum numbers) onto the detector opening (ref. 15); by wobbling the electrostatic sixpole the sharply focused beam is swept in and out the detector opening thereby producing an ac signal proportional to the number of state selected molecules; the broad beam of molecules in states other than the selected state does not contribute to the ac signal. This state selected beam signal is then attenuated by a secondary beam in an external (magnetic or electric) field; the molecules orient themselves with respect to this field direction as quantization axis. The attenuation is measured for the quantization axis parallel and perpendicular to the direction of the (most probable) relative velocity; the relative difference of these signals - the so called anisotropy A - furnishes information on the AIP. The velocity dependence of A shows an undulatory behaviour related to the glory phenomena of the total collision cross section (ref. 21). The amplitude of this anisotropic glory effect can be used to determine the AIP for intermolecular distances $R \approx R_m$.

The strength of the method discussed in this section stems from the fact that for low j-values of the selected state it probes very selectively the P_2-terms of the intermolecular potential (see ref. 5, chapter 3).

In Table 2.2, we have updated the information from ref. 8-21, interpreted in terms of a simple LJ 12-6 potential (Eq. (2.1)). For more refined potential models the reader is referred to the original literature. For H_2-He and H_2-Ne a critical discussion on the sensitivity of A as function of the velocity to changes in the AIP can be found in refs. 14 and 51. In Fig. 2.1 for four NO-noble gas systems a universal plot

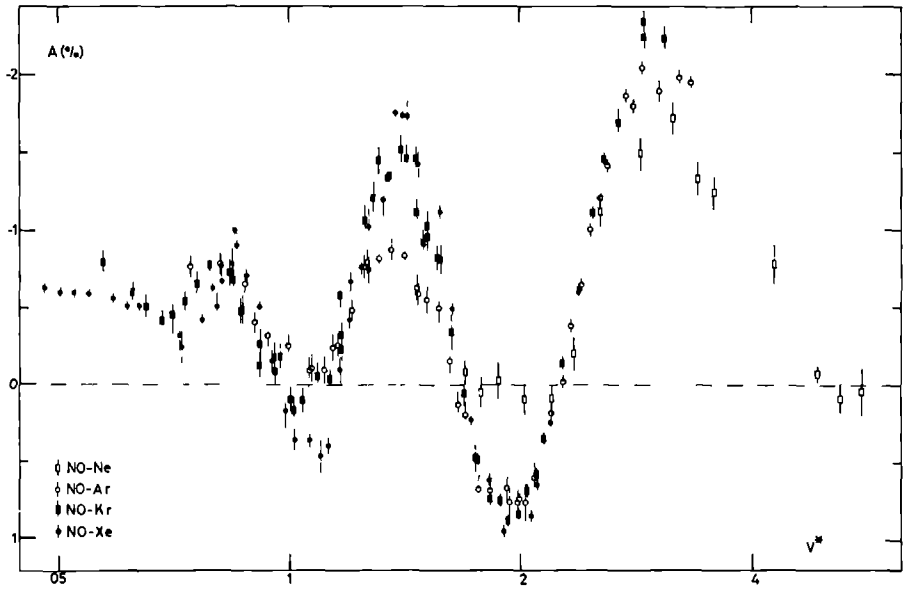

Fig. 2.1. Anisotropy A of NO-Ne, -Ar, -Kr, -Xe vs. the reduced velocity $v^* = \mu v_{rel}/\varepsilon R_m$; A equals the relative difference of the total collision cross section for two orientations of the quantization axis in the scattering region. The glory structure coincides approximately for all systems. However, the damping of extrema is more pronounced for the lighter systems and is attributed to velocity averaging effects. After a correction of about 10% due to the incomplete decoupling of angular momenta, the average value of A yields directly $0.03\ a_0$.

System	ϵ [10^{-14} erg]	r_m [Å]	$\lambda_\perp$	b_0	Ref.
TlF-Ar			0.24 ± 0.01		8
TlF-Kr			.28 ± 0.03		8
TlF-Xe			.16 ± 0.05		8
CsF-Ar			0.355± 0.01		9-11, 21
NO-CO			0.29 ± 0.02		16
NO-CS_2			0.20 ± 0.03		16
NO-N_2O			0.25 ± 0.05		16
NO-N_2			0.21 ± 0.01		20
NO-Ar	1.9	3.6	0.27 ± 0.01	0.7 ± 0.13	
NO-Kr	2.30	3.68	0.22 ± 0.01	0.75 ± 0.03	
NO-Xe	2.81	3.8	0.22 ± 0.01	0.75 ± 0.04	
NO-Ne	1.06	3.10	0.34 ± .1	0.67 ± 0.2	
NO-CO_2			0.14 ± 0.01		15, 16
NO-SF_6			0. 3 ± 0.01		20
H_2-He	0.27	3.01		0.25 ± 0.02	12, 13
				$^{a}B_{\hat{r}} - B_{\hat{r}}$	
H_2-Ne	0.423	3.09	0.17 ± .0	0.35 ± 0.02	12, 13
H_2-H_2	3.34	3.51	0. 8 ± 0.1	0.17 ± 0.02	12, 13
			b_0/a_2		
H_2-Xe	1.24	3.80	0.9 ± 0.1	0.13 ± 0.01	12, 13
H_2-Kr	1.01	3.67	0.9 ± 0.1	0.13 ± 0.01	12, 13
H_2-Ar	1.01	3.43	1.15 ± 0.1	0.16 ± 0.01	12, 13
	ϵr_m [10^{-14} erg Å]				
N_2-N_2	5.24		1.42 ± 0.1	0.11±0.004	14
N_2-CO	5.48		1.34 ± 0.06	0.20± 0.05	14
N_2-Ar	4.2		1.20 ± 0.1	0.145±0.01	14

Table 2.2.

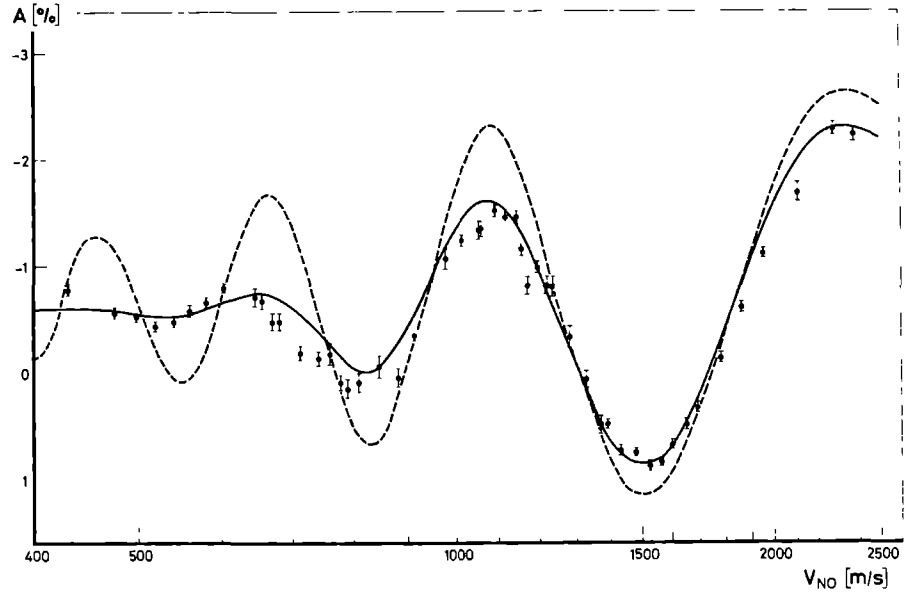

Fig. 2.2. Anisotropy A of NO-Kr vs. the primary beam velocity v_{NO}. The dashed curve gives the theoretical anisotropy in sudden approximation for a LJ 12-6 potential with the parameters of Table 2.2. The solid curve takes into account the velocity distribution of molecules in the primary and secondary beam as well as the effect of incomplete decoupling of angular momenta.

Table 2.2. LJ 12-6 potential fit to anisotropy measurements. The NO-inert gas results correspond to the experimental material depicted in Fig. 2.1 and 2.2. The parameters a_2 and b_2 are defined in Eq. (2.1). For NO-Ne, only preliminary values are shown.

of the anisotropic glory is depicted as function of the reduced velocity $\hbar v_{rel}/\varepsilon R_m$; all systems show a similar pattern except that damping due to kinematic effects of the glory maxima is larger for the lighter collision partners. In Fig. 2.? NO-Kr measurements are compared with the results of a sudden approximation calculation. The kinematic averaging due to the velocity distribution of the molecules in the primary and secondary beam is taken into account. From such a fit the ε-, R_m-, a_2- and b_2 values of Table 2.2 were determined. The b_2-values agree rather well with the ones obtained by an analysis of rotational relaxation of N_2-N_2 by Nyeland and Billing (ref. 53).

Ab initio calculations of the potential surface of H_2-CO can be found in refs. 54 and 55; these theoretical results have not yet been checked against the experimental findings of ref. 12.

Recently, the Na_2-inert gas systems were investigated employing laser fluorescence optical pumping as state selection method (ref. 56); a_2-values ranging from 0.2 to 0.5 have been found.

2.6. DIFFERENTIAL AND INTEGRAL MEASUREMENTS WITH STATE SELECTION, IN NEARLY FORWARD DIRECTION

In this section, some comments are made concerning the differential cross section measurements for polarized, rotationally state selected LiF on Ar by Tsou *et al.* (ref. 57) as well as the state to state inelastic collision measurements in forward direction of TlF and CsF on a large number of collision partners (refs. 58-63). More detailed information can be found in ref. 7. The CsF measurements were theoretically discussed by Dickinson *et al.* (ref. 64).

The very careful analysis of Henrichs et al. (ref. 63) employing different diaphragms to investigate small angle scattering for various angle acceptances yields absolute values for the inelastic transition cross sections. Agreement with theory is obtained for reasonable long range potential parameters.

The main drawback of the inelastic small angle scattering results lies in the fact that mainly long range forces are probed, which (a) are rather well known from perturbative treatments and (b) are quite numerous as consequence of the fact that the convergence of the perturbative series expansion is very slow. Therefore, the information is somewhat poor and difficult to assess.

On the other hand, the LiF-Ar high resolution measurements of ref. 57 show high frequency oscillations of the differential cross section at small angles; one may expect that evaluation of these data will therefore produce information on the ATP for $R \lesssim R_m$ (see for instance ref. 65).

2.7. TOTAL INELASTIC CROSS SECTION USING LASER FLUORESCENCE AND STATE SELECTION

In this section we only mention a recent measurement of the state resolved inelastic cross section for LiH-Ar by Wilcomb and Dagdigian (ref. 66). Their technique consists of a state selected LiH beam of 0.9 eV translational energy focused by means of a 92 cm long four-pole field ($j = 1$, $m_j = 0$ state). Scattering takes place in a scattering chamber where the orientation is assumed to be randomized (no quantization axis, see section 2.5). In this scattering chamber, dye laser

fluorescence is employed to determine molecules in states other than $j = 1$. The laser spot is much smaller than the scattering region so that the integral inelastic cross section is obtained from these measurements by sampling over all angles. A theoretical paper of Bhattacharyya (ref. 67) compares the result of different approximations with the experiment.

2.8. QUENCHING OF GLORY STRUCTURES AND OTHER INTERFERENCE PATTERNS

Glory quenching is an old and venerable theme; the history is reviewed in ref. 19, where especially NO-noble gas systems are discussed. In one of the early papers on this subject, Olson and Bernstein (ref. 68) gave a list of a_2, b_1 and b_2 parameters for LJ 12-6 potentials (Eq. (2.1)) for Li-hydrogen halide systems and Li-NO. The parameters b_1 and b_2 are to be understood as upper limits. We reproduce here the data because the values of the anisotropy parameters look interesting in comparison with those of Table 2.2 which are the result of a much better understood and developed analysis; however, the magnitude of the old determination is right. Note that with the assumption $b_1 \approx 0$ for NO the (corrected) upper limit of $b_2 = 0.64$ is really assumed. If one uses $a_2 = 0.22$ (according to the recent results in Table 2.2) the value $b_2 = 0.76$ is found!

In a recent paper, Bauer et al. (ref. 69) investigate the influence of the AIP on the interference pattern of the small angle differential cross section, for H-Cl_2 and H-Br. From comparison with the experiment they conclude that $b_2 \approx 1$, for these systems.

System	a	a_2	b_1	b_2
Li-HCl	0.38	0.12	0.27	0.61
Li-DCl	0.38	0.13	0.27	0.63
Li-HBr	0.38	0.06	0.25	0.46
Li-HI	0.37	0.03	0.27	0.43
LiNO	0.34 0.34	0.16 0.22	(0.25) (0.25)	0.64 0.76

Table 2.3. Glory quenching results from ref. 68. The parameter a^2 is given by $(b_2 - 1.90\ a_2)^2$, for the homonuclear case which applies approximately also to Li-NO; for the heteronuclear case one has $a^2 = 3.6\ a_2^2 - 3.78\ a_2 b_2 + b_2^2 + 1.91\ b_1^2$. If one takes the ertries for a_2 from an independent determination, the values for b_1 and b_2 result as upper limits. For the definition of a_i and b_i see Eq. (2.1). Some values were corrected with respect to those of ref. 68; the last row is added utilizing the a_2-value of the NO-inert gas systems (see Table 2.2). For Li-NO, the b_1-value should vanish in good approximation.

2.9. DIMER SPECTROSCOPY ON MOLECULAR BEAMS

Dimer spectroscopy has become a powerful tool in the determination of the AIP. Some results on the equilibrium structure mainly of mixed dimers are collected in Table 2.4; much more detailed information can be found in the original literature. In ref. 35, Holmgren et al.

System	Equilibrium structure	Ref.
$(HF)_2$	$\langle R_{FD} \rangle = 1.92$ Å, $\langle \theta_{HF} \rangle = 63^\circ$	22
$(H_2O)_2$	$\langle R_{OO} \rangle = 2.98$ Å, $\langle \theta_1 \rangle = 58^\circ$ $\langle \theta_2 \rangle = -51^\circ$	23,24
HF-HCl	$\langle R_{FH} \rangle = 2.12$ Å; $\langle \theta_{HF} \rangle = 50^\circ$	25
HCN-HF		26
HF-H_2O	$\langle R_{OF} \rangle = 2.68$ Å, $\langle \theta_{HF} \rangle = 0$	27
HF-ClF	$\langle R_{FCl} \rangle = 2.76$ Å, $\langle \theta_{HF} \rangle = 55^\circ$	34
Ar-HCl	$\langle R_{ArH} \rangle = 2.72$ Å; $\langle \theta_{HCl} \rangle = 0$ $a_2 = 0.12$, $R_m = 3.36$	28,33,35
Ar-ClF	$\langle R_{ArCl} \rangle = 3.33$ Å; $\langle \theta_{ClF} \rangle = 0$	29
Ar-HF	$\langle R_{ArH} \rangle = 2.62$ Å; $\langle \theta_{HF} \rangle = 0$	30
Ar-OCS	$\langle R_{CAr} \rangle = 3.58$ Å, $\langle \theta OCAr \rangle = 82^\circ$	31
Kr-ClF	$\langle R_{KrCl} \rangle = 3.39$ Å, $\langle \theta_{ClF} \rangle = 0$	32

Table 2.4. Results of dimer spectroscopy. For $(H_2O)_2$, θ_1 and θ_2 correspond to the angle between the monomer bisectrice of monomer (1) and (2) and the O-H-O axis. In the text is indicated how relations between the anisotropy parameters can be derived from the entries.

attempt to parameterize their results on Ar-HCl in terms of a potential given by our Eq. (2.4) with $\lambda \leq 2$. Sophisticated potential models are explicitly discussed, their potential II (b) yields $a_1 = 0.74$ and $a_2 = 1.07$, the latter one being much larger than the theoretical long range value 0.07. For the relevant information on the repulsive branch of the

potential the reader is referred to the original paper. It would be an important advance to measure this system Ar-HCl with the techniques described in section 2.4 or 2.5 to probe the potential for distances different from those relevant for dimer spectroscopy investigations.

If the data of Harris et al. (ref. 31) on the equilibrium structure of Ar-OCS are analyzed in terms of a LJ 12-6 potential of the form of Eq. (2.1) one obtains the anisotropy parameters $b_1 = 0.67$ and $b_2 = 1.05$ (ref. 70). Here we have used $a_1 = 0$, $a_2 = 0.26$ (from Raleigh light depolarization measurements (ref. 71)) and $R_m = 4.23$ Å (from combination rules). The derivatives of the LJ potential with respect to R and O are put zero for the equilibrium configuration. Similar considerations can be applied to other systems of Table 2.4.

The magnetic beam resonance method is presently applied to $(H_2)_2$ (ref. 72). Fourteen lines were measured for ortho-para and ortho-ortho pairs, partially with very high resolution employing the Ramsey double coil technique. The results are interpreted in terms of a V_2-contribution to the AIP.

Besides for these beam results a rather large effort is undertaken, both experimentally and theoretically, in order to extract information from low temperature - high pressure collision induced ir spectroscopy - where the presence of dimers manifests itself in the occurrence of fine-structured spectra revealing the end-over-end rotational levels of the dimer. The situation is reviewed by Ewing (ref. 73) and Howard (ref. 74). The results for H_2-inert gas dimers are thoroughly discussed in ref. 14. Of later date, although not entirely up to date with respect to the experimental results discussed in section 2.5, is a paper by Dunker and Gordon (ref. 75). LeRoy and co-workers (ref. 76) are engaged

in the work of analyzing simultaneously both the dimer spectroscopic data of McKellar and Welsh (refs. 77 and 78) and the results of ref. 14, anew (ref. 79).

REFERENCES

1. A.T. Amos and R.J. Crispin, in Theoretical Chemistry, Advances and Perspectives (H. Eyring and D. Henderson, Eds.), (Academic Press, New York, 1976)
2. J.G. Stamper, in Theoretical Chemistry 2 (R.N. Dixon and C. Thomson, Eds.), (The Chemical Society, Burlington House, London, 1975)
3. W. Kutzelnigg, Far.Disc. 62 (1977) 185
4. F. Mulder, thesis, Katholieke Universiteit, Nijmegen, The Netherlands (1978)
5. Atom-Molecule Collision Theory: A Guide for the Experimentalist, Contributors: W.R. Gentry, D.J. Kouri, P.J. Kuntz, J.C. Light, M.D. Pattengill, H. Pauly, J. Reuss, H.F. Schaefer III, D. Secrest, S. Stolte (R.B. Bernstein, Eds.), (Plenum, New York, 1979)
6. A.S. Dickinson, Comput.Phys.Commun., to be published
7. M. Faubel and J.P. Toennies, in Advan.Atom.Mol.Phys. 13 (D.R. Bates, Ed.), (Academic Press, New York, 1977)
8. H.G. Bennewitz, K.H. Kramer, W. Paul and J.P. Toennies, Z.Phys. 177 (1964) 84
9. H.G. Bennewitz, R. Gengenbach, R. Haerten and G. Müller, Z.Phys. 226 (1969) 279
10. H.G. Bennewitz and R. Haerten, Z.Phys. 227 (1969) 399
11. H.G. Bennewitz, R. Haerten and G. Müller, Z.Phys. 226 (1969) 139
12. L. Zandee, J. Verberne and J. Reuss, Chem.Phys. 26 (1977) 1
13. L. Zandee and J. Reuss, Chem.Phys. 26 (1977) 327

14. L. Zandee and J. Reuss, Chem.Phys. 26 (1977) 345

15. S. Stolte, J. Reuss and H.L. Schwartz, Physica 57 (1972) 254

16. S. Stolte, J. Reuss and H.L. Schwartz, Physica 66 (1973) 211

17. H.L. Schwartz, S. Stolte and J. Reuss, Chem.Phys. 2 (1973) 1

18. S. Stolte, thesis, Katholieke Universiteit, Nijmegen, The Netherlands (1972)

19. D. Klaassen, H. Thuis, S. Stolte and J. Reuss, Chem.Phys. 27 (1978) 107

20. H.P.M. Kessener and J. Reuss, Chem.Phys.Lett. 31 (1975) 212

21. J. Reuss, in Advan.Chem.Phys. XXX (K.P. Lawley, Ed.), (John Wiley, New York, 1975)

22. T.R. Dyke, B.J. Howard and W. Klemperer, J.Chem.Phys. 56 (1972) 2442

23. T.R. Dyke, K.R. Mack and J.S. Muenter, J.Chem.Phys. 66 (1977) 498

24. T.R. Dyke, J.Chem.Phys. 66 (1977) 492

25. K.C. Janda, J.M. Steed, S.E. Novick and W. Klemperer, J.Chem. Phys. 67 (1977) 5126)

26. A.C. Legon, D.J. Millen and S.C. Rogers, Chem.Phys.Lett. 41 (1976) 137

27. J.W. Bevan, A.C. Legon, D.J. Millen and S.C. Rogers, J.Chem.Soc. Chem.Commun. (1975) 341

28. S.F. Novick, P. Davies, S.J. Harris and W. Klemperer, J.Chem. Phys. 59 (1973) 2273

29. S.J. Harris, S.E. Novick, W. Klemperer and W.E. Falconer, J.Chem. Phys. 61 (1974) 193

30. S.J. Harris, S.E. Novick and W. Klemperer, J.Chem.Phys. 60 (1974) 3208

31. S.J. Harris, K.C. Janda, S.E. Novick and W. Klemperer, J.Chem. Phys. 63 (1975) 881

32. S.E. Novick, P. Davies, S.J. Harris and W. Klemperer, Can.J.Phys. 53 (1975) 2007

33. S.E. Novick, K.C. Janda, S.L. Holmgren, M. Waldman and W. Klemperer, J.Chem.Phys. 65 (1976) 1114

34. S.E. Novick, K.C. Janda and W. Klemperer, J.Chem.Phys. 65 (1977) 5115

35. S. Homgren, M. Waldman and W. Klemperer, J.Chem.Phys. 69 (1978) 1661

36. U. Buck, F. Gestermann and H. Pauly, Chem.Phys. to be published

37. U. Buck, F. Gestermann and H. Pauly, Chem.Phys.Lett. 33 (1975) 486

38. U. Buck, V. Khare and M. Kick, Mol.Phys. 35 (1978) 65

39. J. Schleusener, MPI 5/1978, Göttingen, Germany

40. R. Viard, thesis, Technische Universität, Hannover, Germany (1974)

41. A.R. Blythe, A.E. Grosser and R.B. Bernstein, J.Chem.Phys. 41 (1964) 1917

42. H.J. Loesch, Chem.Phys. 18 (1976) 431

43. G.A. Parker, R.L. Snow and R.T. Pack, J.Chem.Phys. 64 (1976) 1668

44. J.M. Farrar, A.L.J. Burgman, J.M. Parson, R.B. Walker and Y.T. Lee, Lawrence Berkeley Laboratory report 1977/6214

45. U. Buck, F. Huisken and J. Schleusener, J.Chem.Phys. 68 (1978) 5654

46. U. Buck, F. Huisken, J. Schleusener and H. Pauly, Phys.Rev.Lett. 38 (1977) 680

47. W.R. Gentry and C.F. Giese, J.Chem.Phys. 67 (1977) 5389

48. W.R. Gentry and C.F. Giese, Phys.Rev.Lett. 39 (1977) 1259

49. K. Bergmann, Phys.Rev.Lett. 40 (1978) 1447

50. J. Schäfer and W. Meyer, MPI-PAF/Astro 152 (1978), München, Germany

51. K.T. Tang and J.P. Toennies, 68 (1978) 5501

52. U. Buck, private communication

53. C. Nyeland and G.D. Billing, Chem.Phys. 30 (1978) 401

54. J. Prissette, F. Kochanski and D.R. Flower, Chem.Phys. 27 (1978)

55. D.R. Flower, J.M. Launay, E. Kochanski and J. Prissette, to be publised in Chem.Phys.

56. C.A. Linse, thesis, Rijksuniversiteit Leiden, The Netherlands, (1977)

57. T.Y. Tsou, D. Auerbach and L. Wharton, Phys.Rev.Lett. 38 (1977) 20

58. J.P. Toennies, Z.Phys. 182 (1965) 257

59. U. Borkenhagen, H. Malthan and J.P. Toennies, Chem.Phys.Lett. 41 (1976) 222

60. H. Malthan, MPI 16/1976, Göttingen, Germany

61. U. Borkenhagen, MPI 1/1977, Göttingen, Germany

62. U. Borkenhagen, H. Malthan and J.P. Toennies, to be published in J.Chem.Phys.

63. J.M. Henricks, R.P.M. de Bie, C.G.H. Simons and N.F. Verster, VI Int.Symp.Mol.Beams, Noordwijkerhout 1977; private communication

64. A.S. Dickinson and D. Richards, J.Phys.B 6 (1978) 1085

65. K.A. Reed and L. Wharton, J.Chem.Phys. 66 (1977) 3399

66. E.E. Wilcomb and P.J. Dagdigian, J.Chem.Phys. 67 (1977) 3829

67. R S. Bhattacharyya, A.S. Dickinson and D. Richards, to be published

68. R.E. Olson and R.B. Bernstein, J.Chem.Phys. 50 (1969) 246

69. W Bauer, K. Shobatak, J.P. Toennies and K. Walaschewski, J.Chem Phys. 68 (1978) 3413

70. C. Dreyfus, L. Berreby, F. Dayan and J. Vincent-Geisse, J.Chem. Phys. 68 (1978) 2630

71. H. Baas and K. v.d. Hout, to be published

72. J. Verberne and J. Reuss, in Proc XIth Int.Symp.Rarefied Gas Dynamics (R. Campargue, Ed.), (Commissariat à l'Energie Atomique, Paris, 1979)

73. G E. Ewing, Can.J.Phys. 54 (1976) 487,
B.L. Blaney and G.E. Ewing, Ann.Rev.Phys.Chem. 27 (1976) 553

74. B.J. Howard, in Molecular Structure and Properties, Physical Chemistry II, 2 (A.D. Buckingham, Ed.), (Butterworth, London, 975)

75. A M. Darker and R.G. Gordon, J.Chem.Phys. 68 (1978) 700

76. R.L. LeRoy, J.S. Carley and J F. Graberstetter, Far.Disc. 62 (1977) 169

77. A.R.W. McKellar and H.L. Welsh, J.Chem.Phys. 55 (1971) 595

78. A R.W. McKellar and H.L Welsh, Can.J.Phys. 50 (1972) 1158

79. R.J. LeRoy, private communication

CHAPTER 3

INVESTIGATION OF THE ANGLE DEPENDENT PART OF THE INTERMOLECULAR POTENTIAL OF NO-INERT GAS SYSTEMS USING CROSSED MOLECULAR BEAMS

SUMMARY

The relative difference in the total collision cross section for two different orientations of state selected NO ($\Pi_{3/2}$) is examined over a wide velocity range, for the purposes of deriving information on the angle dependent part of the intermolecular potential. The potential parameters for a LJ 12-6 model, ε, R_e, $c_{2,6}$ and $c_{2,12}$ are determined for the systems NO-Ne, -Ar, -Kr, and -Xe.

3.1. INTRODUCTION

Little information is available about orientationally dependent terms in the intermolecular potential (I.P.) at distances which roughly correspond to the position of the potential minimum. In this study the method of state selecting molecules is employed, measuring the total collision cross section for two preferential orientations. A survey of this method and previous measurements can be found in ref. 1.

The experiments of this paper are performed on the NO-inert gas systems, where NO is the molecule to be state selected. Our choice was motivated especially by the paramagnetism, which allows preferential orientation of NO by magnetic fields at moderate strength. On the one

hand the electric dipole moment of NO permits state selection with a very efficient electrostatic multipole focuser, on the other hand the dipole moment is small enough to be neglected in the analysis of our measurements (ref. 2a).

Although the NO-molecule has already a rather complicated structure, possessing an unpaired electron in a Π-orbital and a nearly degenerate pair of I.P.'s (V_Σ and V_Π) in its interaction with an inert gas atom, we perform the analysis with a very simple single potential surface of the form $V_0 + V_2 P_2(\cos\vartheta)$. Here P_2 is the second order Legendre polynomial depending on the angle ϑ between the molecular axis and the intermolecular position vector.

The aim of our experiment is, then, to gather information of the $V_2(R)$ factor of the angle dependent part of the intermolecular potential (A.I.P.). This term is relevant for rotational relaxation and excitation processes. Little is known of the A.I.P. except the old and limited measurements of ref. 2 and some theoretical work of Nielson et al. (ref. 3).

The isotropic part of the intermolecular potential (I.I.P.) is rather unknown, too. Simple combination rules and properties of the pure systems allow an approximate prediction of the depth ε and the position R_e of the I.I.P. (the H-set of ref. 2d). From our meaurements we are able to determine the product εR_e rather accurately, confirming the approximate validity of the H-set parameters.

The experimental method can be explained with the help of Fig. 3.1. State selecting is effected with a 1.6 m long sixpole by which molecules in the $j = \Omega = m_j = 3/2$ state are focused on the detector slit. The two pairs of magnet coils surrounding the secondary beam allow to

choose the quantization axis parallel and perpendicular to the direction of the relative velocity. The attenuation of the beam signal due to the molecules in the selected state is translated into the total cross sections $\sigma_{\parallel}$ and $\sigma_{\perp}$ for these two orientations. The average value of these two quantities (which differ less than 2%) is called $\bar{\sigma}$.

By our measurements we determine the anisotropy A

$$A = (\sigma_{\parallel} - \sigma_{\perp})/\bar{\sigma} \qquad (3.1)$$

A displays a nearly constant average behaviour A_{ng} on which a glory undulation A_g is superimposed.

In section 3.2 the changes of the apparatus are discussed with respect to the previously described version (ref. 2a). The uncorrected experimental results are condensed into a universal plot.

In section 3.3 the theoretical method is indicated by which the measurements are analyzed.

In section 3.4 the corrections of our raw data are discussed, which amount to 50% of the measured A, under the most unfavourable conditions.

In section 3.5 our results are translated into potential parameters.

3.2. EXPERIMENT

3.2.1. TECHNICAL DETAILS

The apparatus was essentially the same as the one used by Stolte et al. (ref. 2). Because the main objective was the extension of the

velocity range, we had to modify the sixpole, the source and the velocity selector as will be described thoroughly in the following. Furthermore, the Rabi-magnet by which on/off modulation of the signal of molecules in the selected state was obtained in the earlier measurements, was replaced. The same goal was achieved by moving the sixpole between two positions: in one position the centre of the focal spot coincides with the detector slit, in the second position the spot occurs laterally displaced by about the spot width (Fig. 3.1). This wobbling sixpole

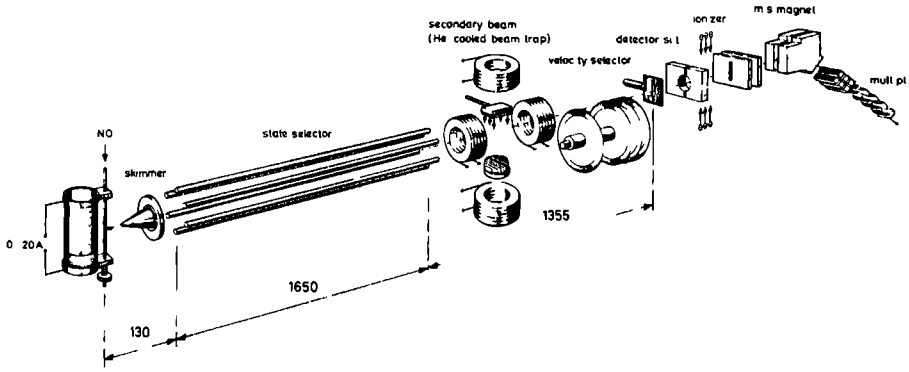

Fig. 3.1. The NO-machine. The NO beam effuses from a 2 mm Ø capillary that can be heated by a direct current, the larger pipe is water cooled, a skimmer is placed 10 mm downstream, the electrostatic sixpole focuses the NO-molecules in the $^2\Pi_{3/2}$ ($J = \Omega = m_J = 3/2$) state onto the detector slit, the scattering region is surrounded by two pairs of coils to produce a B-field of variable orientation, it is pumped cryogenically, the $\Delta v/v = 5\%$ velocity selector is placed between the scattering region and the MV-detector section to shield this section from the secondary beam molecules, distances are indicated in mm, being 1050 mm from the scattering region to the detector slit.

offers two advantages: first, the full acceptance angle of the sixpole can be used, and second, there no longer occurs a pressure build-up at the curved pole faces of the Rabi-magnet which formed a badly pumped region near the source.

In order to obtain focusing at larger velocities either the sixpole dimensions of ref. 2 scaled down such that instead of rod diameter a = 7 mm we worked with a = 5 mm and a = 4 mm or the length of the sixpole was increased to 1600 mm with a = 4 mm. (The unobstructed diameter of the sixpole amounts to 2a.) The new sixpole arrangement enables us to work with velocities up to 2500 m/s, corresponding to 1.0 eV.

The wobbling was achieved by a rotating shaft (2.5 Hz) mounted along side the sixpole with a replacable excenter on each end, by which the angular displacement could be accurately controlled. On the same shaft a pick-up device is mounted which produces the reference input for the lock-in detection.

The liquid nitrogen cooled source of ref. 2 was replaced by a high temperature one, consisting of a stainless steel capillary (inner diameter 1.5 mm, outer diameter 2 mm, length 70 mm). This capillary is mounted vertically under spring tension and can be heated up to 900°C, by direct current passage. In its side wall the source opening has been drilled. The source temperature was derived from the measured velocity distribution of an argon beam.

The velocity selector was adapted to higher velocities by using a massive shaft (ref. 4), on which nine discs were mounted (196 mm diameter, each with 290 slits, 6.5 mm high and 0.9 mm wide). Three discs possess oversized slits to obtain about 45% transmission (ref. 2) for clockwise (+) and counter-clockwise (-) rotation. The rotation frequen-

cy ν is related to the transmitted velocity by v_+ [m/s] = 4.35 ν [Hz] and v_- [m/s] = 8.70 ν [Hz]. The f.w.h.m. yields $[\Delta v/v]_+$ = 5.1% and $[\Delta v/v]_-$ = 11.2%. The maximum used frequency so far is 500 Hz.

The shaft is suspended in ball bearings (MPB type S.R4MCFJHH7). Before being used the bearing are cleaned in an ultrasonic freon bath and run in for about 3 hours at 30 Hz with an excessive amount of microfine molykote powder at atmospheric pressure. During this procedure, which was recommended by the Eindhoven group (ref. 5), the balls assume a blue-black shine.

A new secondary beam source was constructed for the use of the multichannel effuser at 20 K. This low temperature is needed for neon and other light systems, to obtain good kinematic conditions (a well defined relative velocity with respect to both direction and magnitude). The multichannel array consists of two 15 mm diameter stainless steel microfilters with a channel length of 1 mm and diameter 0.018 (Collimated Hole Structure, Brunswick Corporation). This array is mounted on a small reservoir which is connected to a liquid helium cooled surface by a heatpipe and auxiliary graphite rods. The heatpipe mainly serves to obtain short cooling down periods.

For neon at 20 K the pressure in the inlet side of the array amounts to $\sim 10^{-2}$ torr, to obtain a beam attenuation by a factor of 2. The gasload is pumped by a very efficient cryopump as described in ref. 2.

3.2.2. AUXILIARY MEASUREMENTS

It would have been advantageous to work with a nearly monoenergetic

primary nozzle beam in order to minimize intensity losses due to velocity selection. However, we observed that the cooling of the translational degrees of freedom was always accompanied by cooling of the electronic degree of freedom (transition from $^2\Pi_{3/2} \rightarrow {}^2\Pi_{1/2}$). For a large source pressure, these transitions more than off-set the gain from narrowing the velocity distribution. We found an optimum for slight supersonic expansion. For instance, at T_{source} = 300 K and for P_{source} = 10 torr and a nozzle diameter of 200 μ, we have $\Delta v/v \approx 0.4$. The seeding technique was used in combination with a heated source in order to obtain high beam velocities.

The sixpole focuses molecules in the selected state such that an image of the source opening is formed at the plane of the detector slit, with a spot width (f.w.h.m.) of 1.3 mm. This spot is laterally displaced by the wobbling of the sixpole, typically by about D = 1.3 mm. Consequently, it was concluded that also at the highest used velocity the good quality of the focusing was maintained. Within the range $1.2 \leq D \leq 2.2$ mm, we have tested experimentally that the measured anisotropy is unaffected by the magnitude of the lateral displacement.

The phase difference between the isotropic and anisotropic glory was tested by total collision cross section measurements with an unselected NO-beam (for NO-Ar, see Fig. 3.2). Moreover, these measurements are important for the attribution of the correct glory number N to the observed anisotropic glory extrema ($N = 1\frac{1}{4}, 1\frac{3}{4}, 2\frac{1}{4}, 2\frac{3}{4}, 3\frac{1}{4}, 3\frac{3}{4}$). These measurements led to the conclusion that the M-set of potential parameters of ref. 2d should be preferred above the L-set.

The anisotropy depends sensitively on the distribution of the relative velocity (v_{rel}). For the system NO-Ar, the mean velocity of the

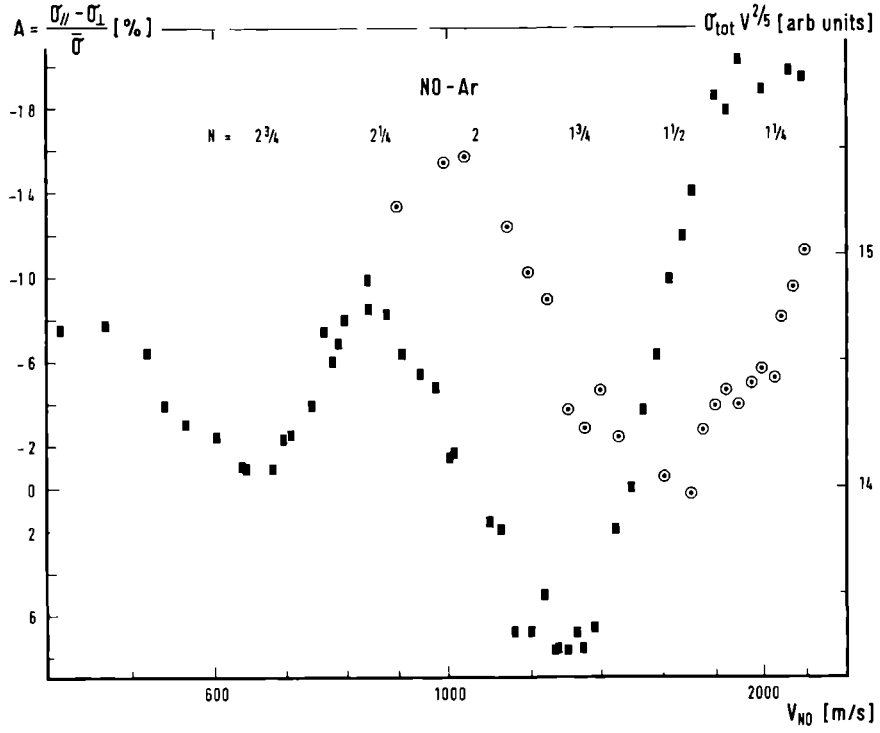

Fig. 3.2. The anisotropy (■) and the total collision cross section (⊙) for NO-Ar versus the primary beam velocity. Note that the extrema of the total cross section coincide with the crossing of the anisotropy with its average value, i.e. a phase shift of about $\pi/2$ is observed.

secondary beam molecules is comparable to the lowest NO-velocity. Therefore, the large angular spread ($\pm$ 20°) of the effusive secondary beam causes a considerable variation of the directions of the relative velocity with respect to the direction of the applied magnetic field B. Moreover, the Maxwellian distribution of the secondary beam molecules give rise to additional averaging effects. We have incorporated the

velocity averaging in a computer program which starts from theoretical anisotropy values and yields the damped anisotropy glories (ref. 6). This damping is discussed in detail in section 3.4.

The measurements of the anisotropy were done with one attenuation (a factor 3) at all velocities for all systems (except for Ne where it was a factor 2), i.e. the pressure in front of the multichannel array was increased for the high velocity measurements in order to obtain this 1/3 (or 1/2) attenuation.

3.2.3. UNIVERSAL PLOT

In Fig. 3.3 all our inert gas anisotropy results are shown as a function of the reduced velocity $v^* = \hbar v_{rel}/\varepsilon R_e$. In this expression ε and R_e stand for the depth and the position of the minimum of the isotropic part of the potential. For a certain potential (for instance LJ 12-6) fixed glory number N occur at fixed v_N values ($v_{3\frac{1}{4}}$, $v_{2\frac{3}{4}}$, $v_{2\frac{1}{4}}$, $v_{1\frac{3}{4}}$, $v_{1\frac{1}{4}}$).

The oscillations disappear for small velocities, due to a damping (influence of velocity distribution). The same effect is suggested for the fixed glory number $N = 2\frac{1}{4}$; the amplitude increases going from argon to krypton to xenon.

A decrease of glory amplitudes for decreasing velocities (increasing glory numbers N) comes also from theory through variations of the glory phase shift for different orientations compatible with a chosen quantization axis (direction of the B-field in the scattering region): although a well defined state is selected one deals with a distribution of molecular orientations; the observed effect probes the average over

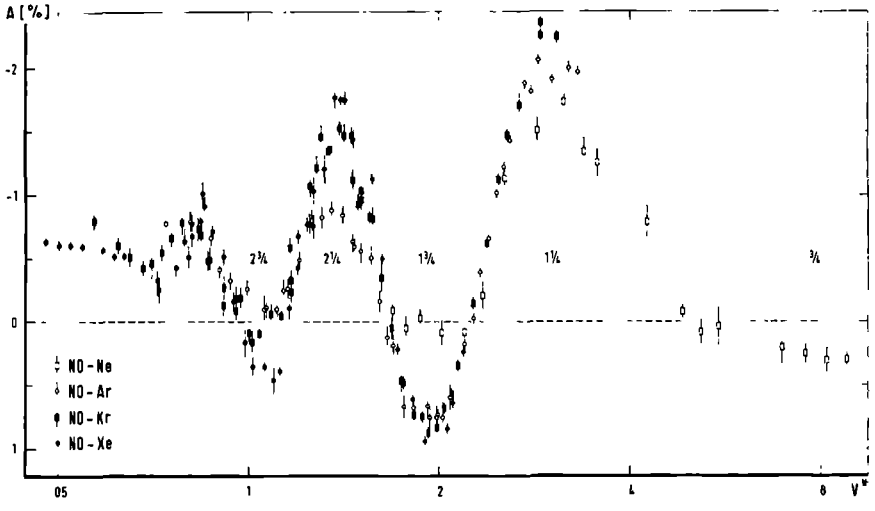

Fig. 3.3. Anisotropy results versus the reduced velocity $v^* = \mu v_{rel}/\epsilon R_e$, for NO-inert gas systems. At the positions of the extrema the glory number N is indicated. The differences in amplitude (for instance at N = 2¼) show the larger damping for the lighter systems due to less favorite kinematic conditions. The values for ϵ and R_e are taken from Table 3.1. The old experimental points of ref. 2d are included.

this distribution. For large glory phase shifts ($\eta_{glory} = \pi[N - 3/8]$ for $v = v_N$) this quantum mechanical distribution leads to significant quenching of glory amplitudes through higher order contributions.

From this universal plot we can derive the product ϵR_e in the LJ 12-6 potential model for the investigated systems (see Table 3.1). Attribution of the glory number N was guided by a Bernstein plot (ref. 7) and by our measurement of the isotropic glory behaviour.

In comparison with the work of Zandee et al. (ref. 8a, 8b, 8c, es-

System	εR_e (exp) 10^{-14} Å erg	εR_e^6 (exp) 10^{-10} Å^6 erg	εR_e^6 (theor) 10^{-10} Å^6 erg	ε 10^{-14} erg	R_e Å	$q_{2,6}$	$q_{2,12}^{-1.5}q_{2,6}$
NO-Ne	3.11(3)		0.31	1.06(3)	3.11(6)	0.40(4)	0.25(5)
NO-Ar	6.91(3)	0.42(3)	0.42	1.91(3)	3.62(6)	0.30(3)	0.20(4)
NO-Kr	8.45(3)		0.57	2.30(3)	3.68(6)	0.30(3)	0.20(4)
NO-Xe	10.15(3)		0.80	2.68(3)	3.79(6)	0.30(3)	0.20(4)

Table 3.1. Survey of the potential parameters for the LJ 12-6 model. For all systems ε, R_e, $q_{2,6}$ and $q_{2,12}$ could be determined making use of the theoretical values of εR_e^6 as obtained from the Slater-Kirkwood relation which was tested for NO-Ar (section 3.5.2). All systems, except for NO-Ne, show the same anisotropy.

pecially Fig. 4.1 in ref. 8a) most of our measurements fall into the glory region. However, for the neon system we were able to probe also the transition region.

3.2.4. ABSOLUTE VALUES OF THE TOTAL COLLISION CROSS SECTION

Recently, absolute values for the total collision cross section were reported for O_2-noble gas systems (ref. 9). We compared beam attenuations for equal secondary beam conditions, with O_2 and NO as primary beam molecules. From these measurements, εR_e^6-values were extracted, which are compared with the Slater-Kirkwood values in section 3.5.2.

3.3. THEORY

3.3.1. THE POTENTIAL

The interaction between NO and its scattering partners is described by

$$V = V_0(R) + V_2(R)P_2(\cos\Theta)$$

$$= \epsilon\left[\left(\frac{R_e}{R}\right)^{12} - 2\left(\frac{R_e}{R}\right)^{6}\right] + P_2(\cos\Theta)\left[q_{2,12}\left(\frac{R_e}{R}\right)^{12} - 2q_{2,6}\left(\frac{R_e}{R}\right)^{6}\right] \qquad (3.2)$$

Here $q_{2,12}$ and $q_{2,6}$ are the so called anisotropy parameters. The angle dependence is given by the second order Legendre polynomial $P_2(\cos\Theta)$, where the angle Θ is formed by the molecular axis (direction $\hat{r}$) and the vector between the centres of the colliding systems (direction $\hat{r}'$).

This potential represents a simplification to the real problem, because higher order Legendre polynomials are neglected (proportional to P_{2n} with $n > 1$) and because the excentricity of NO is disregarded (i.e. Eq. (3.2) does not contain Legendre polynomials of odd order, P_{2n+1}). Furthermore, terms that describe a deperdence of the interaction on a rotation of the NO molecule around its molecular axis are neglected. This effect is contained in the potential model used by Poppe (ref. 10)

$$V = V_0(R) + P_2(\cos\Theta)V_2(R) + [Y_{2,2}(\Theta,\Phi) + Y_{2,-2}(\Theta,\Phi)]V_2(R) \qquad (3.3)$$

Due to the fact that all three neglected terms (proportional to P_{2n} with $n > 1$; P_{2n+1}; Y_{2m}) only contribute in higher order calculations

and that the first order distorted wave approximation (dwa) and the first order sudden approximation seems to describe the measured anisotropy A at least at high velocities (ref. 11), we feel justified to use the simple potential model of Eq. (3.2). Moreover, Nielson et al. (ref. 3) have estimated that the strength of the $Y_{2m'}$-term is less than 15% of the P_2-term. The important point is that in lowest order only terms with $q_{2,12}$ and $q_{2,6}$ remain, i.e. that our anisotropy measurements single out the term proportional to $P_2(\cos\theta)$.

3.3.2. THE ANISOTROPY IN SUDDEN APPROXIMATION

The theoretical discussion is based upon sudden approximation (sa) (ref. 11,12) which takes into account, at least in an approximate way, higher order effects of the anisotropic term in Eq. (3.2). The total collision cross section, $\sigma(\beta)$, for an anisotropic potential of the form $V = V_0 + V' = V_0 + V_2 P_2(\cos\theta)$ is given by ref. 12

$$\sigma_{tot}(\beta) = \int_0^\infty b\,db \int_0^{2\pi} d\varphi' \{2 - 2\langle\beta|\cos(2\eta_1 - 2\delta_1)|\beta\rangle\} \qquad (3.4)$$

For NO, symmetric top eigenfunctions were adopted (ref. 13)

$$|\beta\rangle = (-)^{m_j - \Omega} \sqrt{\frac{2j+1}{8\pi^2}}\, D^j_{m_j}(\varphi, \vartheta, \gamma) \qquad (3.5)$$

Actually, linear combinations with $\Omega = \pm|\Omega|$ are strictly required; however, since the following calculations depend solely on $|\Omega|$ this feature is omitted. The quantum number m_j is defined with respect to the direction of the relative velocity. The impact parameter b is related

to the orbital quantum number $bk = l + \frac{1}{2}$, where k is the wave number. The angle φ' describes the azimuth angle of the trajectory around the direction of the relative velocity. The phase shifts η_l (derived from the isotropic part of the potential, alone) are accompanied by δ_l which correspond to action integrals

$$\delta_l = \frac{1}{\hbar} \int_0^\infty V'(t')dt' \tag{3.6}$$

There are two regions where η_l does not vary strongly with l (i.e. the non glory region for large impact parameters and the glory region for $b \approx R_e$). Outside these regions the cosine in Eq. (3.4) averages to zero upon integration over b.

For large impact parameters, one may use straight path trajectories with $v_{rel}dt' = RdR/\sqrt{R^2 - b^2}$; the phase shift can be obtained from Born approximation, $\eta_l = (3\pi/16\hbar)(2\varepsilon R_e^6/v_{rel}b^5)$. The quantity $\delta_l << \pi/2$ derives from the long range contribution $V_2 \approx -q_{2,6}(2\varepsilon R_e^6/R^6)$. This leads to the non glory part of the total collision cross section, neglecting higher order terms and assuming the molecular axis to remain space-fixed during the encounter

$$\sigma_{ng}(\beta) = \int_0^\infty bdb \int_0^{2\pi} d\varphi' \{2 - 2\langle\beta|\cos 2\eta_l - 2\delta_l \sin 2\eta_l|\beta\rangle\}$$

$$= 8.083(2\varepsilon R_e^6/\hbar v_{rel})^{2/5}\{1 - \frac{1}{10} q_{2,6}\langle\beta|P_2(\hat{r}.\hat{v}_{rel})|\beta\rangle\} \tag{3.7}$$

The glory part of the total collision cross section is obtained from the second region ($b \approx R_e$) where we use the parabola approximation for the phase shift (ref. 14) $\eta_l = \eta_m - 1/2|\eta_m''|(l - l_m)^2$. Applying the

stationary phase method for the integration over b one finds (ref. 12)

$$\sigma_g(\beta) = -\frac{2l_m}{k^2}\sqrt{\frac{\pi}{|\eta_m''|}}\int_0^{2\pi} d\varphi' \langle\beta|\cos(2\eta_m - \pi/4 - 2\delta_m)|\beta\rangle \qquad (3.8)$$

For η_m and $l_m/\sqrt{|\eta_m''|}$ we use series expansions as function of the reduced energy (ref. 7); further

$$\delta_m = \delta_{l=l_m} = \frac{2R_e\varepsilon}{2^{1/6}\hbar v_{rel}}\{-1/2q_{2,12}S^{(m)}(12,0,0) + 1/2q_{2,6}S^{(m)}(6,0,0) +$$

$$+ 3/2\cos^2\vartheta[q_{2,12}S^{(m)}(12,2,0) - q_{2,6}S^{(m)}(6,2,0)] +$$

$$+ 3/2\sin^2\vartheta\cos^2(\varphi - \varphi')[q_{2,12}S^{(m)}(12,0,2) - q_{2,6}S^{(m)}(6,0,2)]\} \qquad (3.9)$$

Values for the S-integrals can be found in ref. 11, with the definition $S^{(m)}(i,2,0) = S^{(m)}(i,0,0) - S^{(m)}(i,0,2)$. With the quantization axis chosen along the direction of the relative velocity ($\vartheta_B = \sphericalangle(\hat{v}_{rel},\hat{b})=0$) the total collision cross section for a certain state $\sigma(\beta) = \sigma(m_j';\vartheta_B=0)$ can be written

$$\sigma(m_j';0) = \sigma_{ng}(m_j';0) + \sigma_g(m_j';0) \qquad (3.10)$$

where Eqs. (3.5), (3.7) and (3.8) yield

$$\sigma_{ng}(m_j';0) = 8.083\left(\frac{2\varepsilon R_c^6}{\hbar v_{rel}}\right)^{2/5}\left[1 + \frac{1}{10}q_{2,6}\frac{[3m_j'^2 - j(j+1)][j(j+1) - 3\Omega^2]}{(2j+3)(2j-1)j(j+1)}\right] \qquad (3.11a)$$

and

$$\sigma_g(m_j';0) = -(2j+1)\frac{l_m}{k^2}\sqrt{\frac{\pi}{|\eta_m''|}}\int_0^{2\pi} d(\varphi-\varphi')\int_0^{\pi}\sin\vartheta d\vartheta\cos(2\eta_m - \frac{\pi}{4} - 2\delta_m)[d^j_{m_j',\Omega}(\vartheta)]^2$$

(3.11b)

The rotation functions $d^j_{m_j',\Omega}(\vartheta)$ are defined according to Eq. (4.1.15) of ref. 13.

For a different choice of the quantization axis along $\hat{B}$ with $\vartheta_B \neq 0$ we use the general relation (see for instance Eq. (33), chapter 2 of ref. 15)

$$\sigma(m_j;\vartheta_B) = \sum_{m_j'} [d^j_{m_j',m_j}(\vartheta_B)]^2\sigma(m_j';0) \qquad (3.12)$$

Considering NO in the $^2\Pi_{3/2}$ state with $j = m_j = \Omega = 3/2$ one finds

$$\sigma(3/2;\vartheta_B) = \sigma^0 + \frac{1}{2}P_2(\cos\vartheta_B)[\sigma(3/2;0) - \sigma(1/2;0)] \qquad (3.13)$$

Here, use is made of the general property (for instance, ref. 16) $\sigma(m_j',0) = \sigma(-m_j';0)$. Moreover, $\sigma^0 = \frac{1}{2j+1}\sum_{m_j'}\sigma(m_j';0)$ stands for the m_j-averaged cross section corresponding to the situation without state selection. Eqs. (3.6), (3.7) and (3.9) yield $\sigma^0 = \sigma^0_{ng} + \sigma^0_g$, with

$$\sigma^0_{ng} = 8.083\left(\frac{2\pi R_e^6}{\hbar v_{rel}}\right)^{2/5} \qquad (3.14a)$$

$$\sigma^0_g = -\frac{l_m}{k^2}\sqrt{\frac{\pi}{|\eta_m''|}}\int_0^{2\pi} d(\varphi-\varphi')\int_0^{\pi}\sin\vartheta d\vartheta\cos(2\eta_m - \frac{\pi}{4} - 2\delta_m) \qquad (3-14b)$$

The ϑ_B dependent part of Eq. (3.13) contains the factor

$$\sigma(3/2;0) - \sigma(1/2;0) = [\sigma_{ng}(3/2;0) - \sigma_{ng}(1/2;0)] + [\sigma_g(3/2;0) - \sigma_g(1/2;0)],$$

where

$$\sigma_{ng}(3/2;0) - \sigma_{ng}(1/2;0) = -8.083 \cdot \frac{1}{25} \left(\frac{2\varepsilon R_e}{\hbar v}\right)^{2/5} q_{2,6} \qquad (3.15a)$$

$$\sigma_g(3/2;0) - \sigma_g(1/2;0) = -(2j+1)\frac{1}{k^2}\sqrt{\frac{\pi}{|n''_m|}} \int_0^{2\pi} d(\varphi-\varphi') \int_{-1}^{+1} d(\cos\vartheta)\cos(2\eta_m - \frac{\pi}{4} - 2\delta_m)\tfrac{1}{2}P_2(\cos\vartheta) \qquad (3.15b)$$

The term $\frac{1}{2}P_2(\cos\vartheta)$ results from $[d^{3/2}_{3/2,3/2}(\vartheta)]^2 - [d^{3/2}_{1/2,3/2}(\vartheta)]^2$, taking into account that the integrand must be an even function of $\cos\vartheta$.

The anisotropy A is defined as the relative difference between the total collision cross section for two orientations of the quantization axis $\vartheta_{B\parallel}$ and $\vartheta_{B\perp}$ which are chosen to be 0 and $\pi/2$, for the most probable velocity,

$$A = [\sigma(3/2,\vartheta_{B\parallel}) - \sigma(3/2,\vartheta_{B\perp})]/\sigma^0 \qquad (3.16)$$

Again, as the total collision cross section also the anisotropy can be divided into a glory part A_g and a non glory part A_{ng} with

$$A_{g(ng)} = \frac{1}{2\sigma^0}[\sigma_{g(ng)}(3/2;0) - \sigma_{g(ng)}(1/2;0)][P_2(\cos\vartheta_{B\parallel}) - P_2(\cos\vartheta_{B\perp})] \qquad (3.17)$$

This quantity must be averaged over the v_{rel} distribution occurring for a certain setting of the velocity selector and for the pertaining secondary beam condition in order to obtain the actual measured anisotropy. Whether one neglects σ^0_g is of little importance (1% effect in A) in

view of the actual experimental accuracy of this work. The averaging procedure will be discussed in section 3.4.

For the ideal situation of mono-energetic and unidirectional primary and secondary beams one has the fixed values $\vartheta_{B\parallel(\perp)} = 0(\pi/2)$. The anisotropy yields, then

$$A_{ng} = -0.03 q_{2,6} \tag{3.18a}$$

and

$$A_g = \frac{3}{4\sigma^0} [\sigma_g(3/2;0) - \sigma_g(1/2;0)] \tag{3.18b}$$

Remarkably, the non-glory contribution consists of a velocity independent quantity which depends only on $q_{2,6}$. A_{ng} probes the intermolecular potential at $R_{ng} \approx \sqrt{\frac{\sigma^0}{2\pi}}$ with $1.6 R_e \approx 6.4$ Å $< R_{ng} < 8.2$ Å $\approx 2.1 R_e$, for the velocity range investigated.

Concerning A_g the position of the extrema (at $N = 1\frac{1}{4}, 1\frac{3}{4}, \ldots$) mainly depends on V_0 similar to the isotropic glories. The amplitude, however, depends sensitively on V_2 and is approximately zero for the whole velocity range if $q_{2,12}/q_{2,6} = 1.5$ (ref. 11), i.e. the contribution of the attractive part of V_2 (proportional to $q_{2,6}$) has the opposite effect as compared to the repulsive contribution (proportional to $q_{2,12}$).

3.4. CORRECTIONS

3.4.1. KINEMATIC EFFECTS

In Eq. (3.17), evidently the non-glory contribution depends only on the directional distribution of the relative velocity. On the other

hand the glory contribution A_g (Eq. (3.17)) depends on the distribution of both $\hat{v}_{rel}$ and v_{rel}. Here, $v_{rel} = |\vec{v}_{NO} - \vec{v}_2|$. For the most probable velocity of the secondary beam $v_{2,max}$ we have used $v_{2,max} = (2kT_2/m_2)^{1/2}$ = 123 m/s (Xe, T_2 = 120 K); 135 m/s (Kr, T_2 = 90 K); 200 m/s (Ar, T_2 = 90 K); 134 m/s (Ar, T_2 = 55 K); 135 m/s (Ne, T_2 = 21 K). On the average we assume that the primary beam intersects the secondary beam at 90°. The imperfect kinematics due to the velocity distribution of both beams are demonstrated in Table 3.2 and Figs. 3.4a-d. Perhaps surprisingly, the kinematic of Ne is as good as that of Kr because we were able to cool the secondary beam source to a much lower temperature,

		v_{NO} = 400 m/s		v_{NO} = 2400 m/s	
System	T_2 [K]	$\Delta v_{rel}/v_{rel}$	$C_{\hat{v}}$	$\Delta v_{rel}/v_{rel}$	$C_{\hat{v}}$
NO-Ne	21	0.30	0.90	0.081	0.996
NO-Ar	90	0.42	0.85	0.087	0.994
NO-Kr	90	0.27	0.912	0.080	0.997
NO-Xe	120	0.25	0.923	0.078	0.998

Table 3.2. The influence of the distribution (magnitude and direction), of the relative velocity, for two settings of the velocity selector (v_{NO} equals the velocity of maximum transmission); T_2 is the temperature of the target beam; $\Delta v_{rel}/v_{rel}$ gives the f.w.h.m. for the function that describes the probability to find a certain relative velocity v_{rel}; $C_{\hat{v}}$ stands for the kinematic polarization which is practically constant within the range $2\Delta v_{rel}$ (section 3.4.1).

before Ne starts to condense. One should compare to the old measurements of Schwartz et al. (ref. 2), they were performed under the conditions corresponding to the low velocity side of Table 3.2, the improvement of kinematics by the present high velocity measurements is evident.

To calculate the influence of the velocity distributions a very elaborate computer program was developed (ref. 6). This program takes into account that at a certain point in the scattering region the primary beam is bombarded by the secondary beam molecules originating from quite different sections of the effuser (50 mm length and 10 mm width). The surface of the multichannel array is mounted 12 mm above the center of the primary beam, the primary beam has a practically cylindrical shape over the length of the scattering region (4 mm diameter). At a

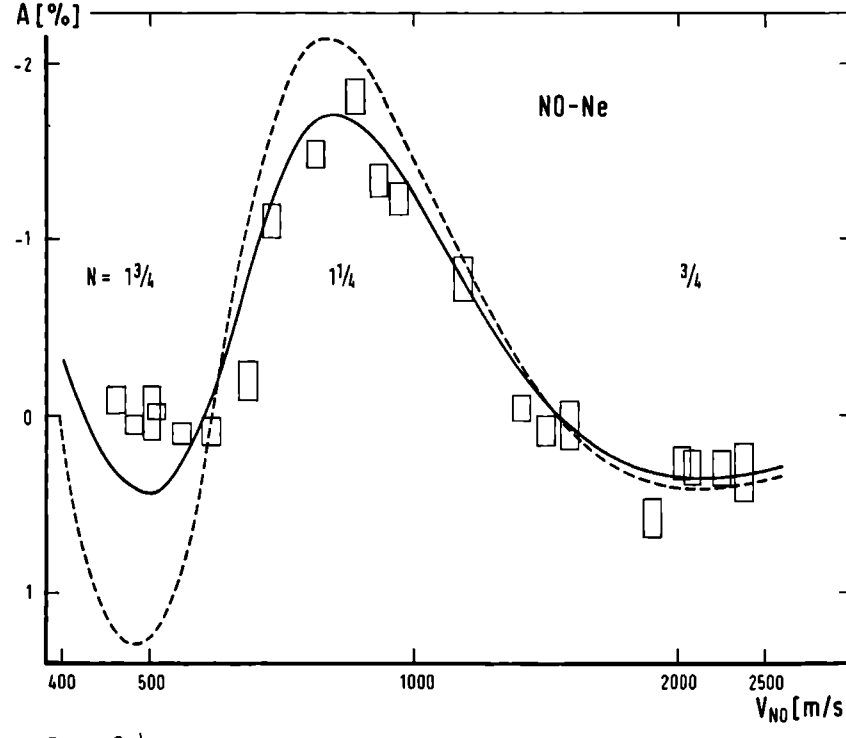

Fig. 3.4a.

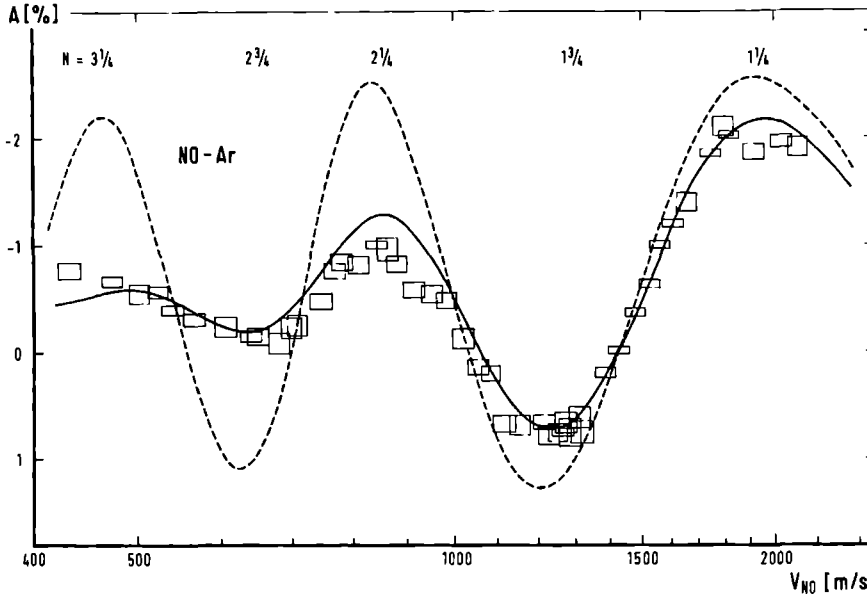

Fig. 3.4b.

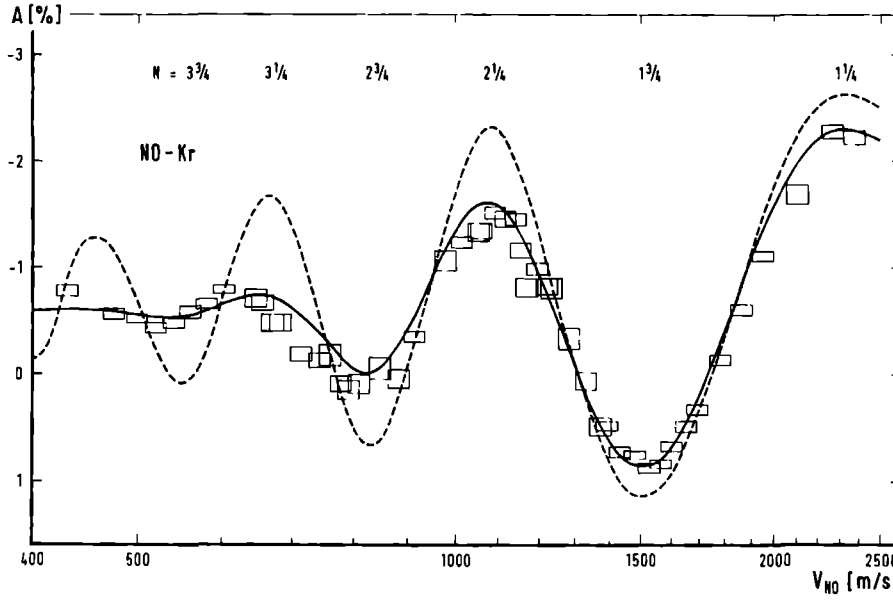

Fig. 3.4c.

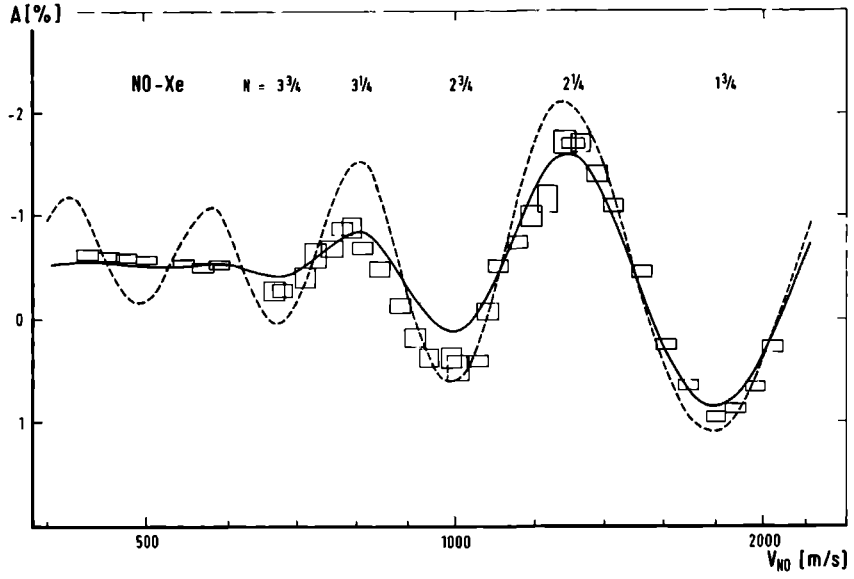

Fig. 3.4a-d. Anisotropy results for a) NO-Ne, b) NO-Ar, c) NO-Kr, d) NO-Xe versus the primary beam velocity. Experimental values are shown with their uncertainty, one standard deviation in vertical direction and 3% in horizontal direction due to the inaccuracy of the calibration of the velocity selector. The dashed curves give the theoretical results (Eq. (3.18) and parameters of Table 3.1 for a LJ 12-6 potential). The solid lines include all corrections of section 3.4.

certain position in the scattering region the primary beam molecules see the scattering partner approach under different angles. Even if one restricts the consideration to a small section of the multichannel array the distribution in magnitudes of the velocity (assumed to be Maxwellian for the secondary beam and triangular for the velocity

selected primary beam) produces a spread in angles.

The angle distribution of the molecules effusing from the multichannel array is assumed according to Zugenmaier (ref. 17). The influences of this assumption were tested by an additional calculation employing a cosine distribution. In an extrema a negligible difference of glory damping was observed, for both distributions.

The correction of A_{ng} reflecting the quantity $C_{\hat{v}}$ (see Table 3.2) amounts to about 15% for lower velocities and becomes negligible for higher velocities. The kinematic polarization $C_{\hat{v}} \leq 1$ is defined as the average value of $3/2[P_2(\cos\vartheta_{B\parallel}) - P_2(\cos\vartheta_{B\perp})]$ (see Eq. (3.17)); the measured $A_{g(ng)}$ is proportional to $C_{\hat{v}}$.

For the glory amplitude A_g, however, the corrections reflect mainly the influence of the velocity spread $\Delta v_{rel}/v_{rel}$ (Table 3.2). This results in a total damping at low velocity and decreases to a 10% effect at the highest velocity.

3.4.2. EFFECTS DUE TO INCOMPLETE DECOUPLING OF ANGULAR MOMENTA

The magnetic field in the scattering region amounts to 150 G. The Zeeman effect of the NO-molecules in the $j = m_j = \Omega = 3/2$ state nearly corresponds to the strong field case. However, the remaining coupling of the nuclear angular momentum to the rotational angular momentum results in a slight mixing of m_j states. This mixing yields a correction factor $C_{B_0} = 0.905$ as was discussed in ref. 2a and 2c. This correction factor applies to both A_{ng} and A_g ($A(\text{observed}) = C_{B_0}.A(\text{theoretical})$).

The finite angular resolution of our machine influences the anisotropy according to

$$C_{\Delta\gamma}.A = \frac{\sigma_{\parallel} - (\int_{\Delta\Omega_a} - \int_{\Delta\Omega'_a}) \frac{d\sigma_{\parallel}}{d\Omega} d\Omega - \sigma_{\perp} + (\int_{\Delta\Omega_a} - \int_{\Delta\Omega'_a}) \frac{d\sigma_{\perp}}{d\Omega} d\Omega}{\bar{\sigma} - (\int_{\Delta\Omega_a} - \int_{\Delta\Omega'_a}) \frac{d\sigma}{d\Omega} d\Omega} \qquad (3.19)$$

$\sigma_{\parallel}$ and $\sigma_{\perp}$ are the total collision cross sections with the quantization axis parallel or perpendicular to the relative velocity; $d\sigma_{\parallel}/d\Omega$ and $d\sigma_{\perp}/d\Omega$ are the corresponding differential cross sections. The solid angle $\Delta\Omega_a$ is defined by the detector opening as it is seen from the scattering region. Similarly $\Delta\Omega'_a$ is defined, but now for the off-axis position of the wobbling sixpole, so that $\Delta\Omega'_a$ has the same magnitude as $\Delta\Omega_a$ but it is centered around a non zero angle.

It is evident from Eq. (3.19) that the angular resolution correction is diminished by the use of the wobbling sixpole as $\Delta\Omega_a$ and $\Delta\Omega'_a$ are nearly equal and as for small angles $d\sigma/d\Omega$ (on axis) $\approx$ $d\sigma/d\Omega$ (off axis). The angles are roughly made equal to the experimental angle resolution; see also section 3.2.2 for test measurements where different wobbling angles were used. For small wobbling angles, however, the signal due to the molecules in the selected state becomes small, so one has to compromise between the signal to noise ratio of the anisotropy measurements and a small angular resolution correction. In practice the displacement of the spot is made about equal to the f.w.h.m. of the spot width (1.3 mm), in the detector plane. The detector slit has a width of 1 mm.

It was shown by a careful calculation (ref. 18) using a semi-

classical differential cross section expression of Verster (ref. 19) that the angular resolution correction is very small in our experiment. For example, the correction for $C_{\Delta\gamma}$ amounts to 0.4% at 500 m/s and 3% at 2000 m/s for the system NO-Ar. We therefore conclude that the correction is negligible and put $C_{\Delta\gamma} = 1$. In ref. 2 the factor was assumed to have a value of about 0.9; the effect was overestimated because the wobbling of the sixpole was not taken into account; i.e. the integral $\int_{\Delta\Omega'_a}$ was neglected.

3.4.4. THE EFFECT OF THE INHOMOGENEITY OF THE FIELD

Two other corrections remain to be discussed; both turn out to be negligible. The magnetic field in the scattering region produced by two pairs of Helmholtz coils shows a variation in strength and in direction along the beam path. Both effects were estimated carefully in ref. 2a and shown to be less than 1% of the anisotropy.

3.5. RESULTS

3.5.1. DETERMINATION OF εR_e

As was discussed in section 3.3, the spacing of the anisotropic glory depends mainly on the properties of V_0, in s.a. Consequently, one can use this information to extract the value of $a_1\varepsilon R_e$ for the different systems and possibly also of $(2\varepsilon^2 R_e/\pi\hbar)A_1$ (ref. 7). Here one has $a_1 = 0.421559$ for an LJ 12-6 potential ($a_1 = 0.47$ for LJ = 8-6) and $A_1 = 0.1655$, the latter one being rather independent of the chosen potential. In Table 3.1 the results of this fit are shown.

3.5.2. DETERMINATION OF εR_e^6

The potential parameter $C_6 \propto \varepsilon R_e^6$ can be found from an experimental determination of the absolute value of the total cross section, see Eq. (3.5). Absolute values were reported by Luzzati et al. (ref. 9) for similar systems: O_2-Ar, -Kr, and -Xe. We have compared the attenuation with Ar as secondary beam under the same conditions, using alternating NO and O_2 as non-state selected primary beam. To get rid of glory effects this comparison took place at various relative velocities. The ratio $\varepsilon R_e^6(NO\text{-}Ar)/\varepsilon R_e^6(O_2\text{-}Ar)$ was found to be 1.038 ± 0.004.

From the well established Kirkwood relation for the long range dispersion coefficient (ref. 20), $C_6 = [(3/2)e^2 a_0^{1/2} \alpha_a \alpha_b]/[(\alpha_a/n_a)^{1/2} + (\alpha_b/n_b)^{1/2}]$, we had for this ratio 1.0500, using $\alpha_{NO} = 1.74$ Å^3, $\alpha_{Ar} = 1.64$ Å^3 and $\alpha_{O_2} = 1.59$ Å^3 (ref. 21), $n_{\text{inert gas}} = 8$, $n_{NO} = 11$ and $n_{O_2} = 12$. This satisfying agreement encouraged us to calculate (instead of measuring) the εR_e^6-ratio for all systems investigated by us. For Ne, Kr and Xe we used (ref. 21) $\alpha_{Ne} = 0.395$ Å^3, $\alpha_{Kr} = 2.48$ Å^3 and $\alpha_{Xe} = 4.04$ Å^3. In Table 3.1, the isotropic potential parameters can be found, obtained from $C_6 = 2\varepsilon R_e^6$ valid for a LJ 12-6 potential. For more realistic potentials, the proportionality factor between C_6 and εR_e^6 can differ from two, yielding about 1.2 for rare gas dimers according to Tang and Toennies (ref. 22). As a consequence the R_e-values should be increased by 11% (ε-values decreased by the same percentage) with respect to the values of Table 3.1.

Without the absolute cross section measurement and without application of the Slater-Kirkwood relation, ε and R_e could not have been independently determined from our investigation.

3.5.3. DETERMINATION OF ANISOTROPY PARAMETERS $q_{2,6}$ AND $q_{2,12}$

In Fig. 3.3, the measured A-values are displayed for NO-Ne, -Ar, -Kr and -Xe. We have succeeded to describe the anisotropy with sa (Eqs. (3.15) and (3.17)) and the corrections of section 3.4. As fit parameters occur εR_e, $q_{2,6}$ and $q_{2,12}$. A uniform value for $q_{2,6}$ has been fitted to all systems leading to the result in Table 3.1. We have chosen this procedure for two reasons. For the heavier noble gases we convinced ourselves that the lowest attainable value for v_{rel}, in the case of NO-Ar, introduces a bias for the calculation of the velocity averaged value of the anisotropy, A_{ng}, resulting apparently in too low a value. The same would occur for the Kr- and Xe-systems if we would have stopped measuring at the same reduced velocity v^* (see section 3.2.3 and Fig. 3.3). The Kr- and Xe-systems yield the same $q_{2,6}$-value if an independent fit is employed. On the other hand, the experimental range of v-values for Ne-NO do not permit an accurate determination of the $q_{2,6}$-value because the anisotropy is measured at the brink of the transition region so that velocity averaging seems not very meaningful a procedure. Therefore, we have adopted the value for $q_{2,6}$ from the Kr- and Xe-systems.

The values of $q_{2,12}-1.5q_{2,6}$ are determined separately for each system with the unexpected result that for the three heavier systems the same value was obtained. The results of such a fit are shown in Figs. 3.4a-d, too. Table 3.1 contains the thus found potential parameters. For χ^2 we found values about four times the number of measurements, using the statistical error of the individual measurements (1 standard deviation).

The uncertainty of the potential parameters in Table 3.1 corresponds to a change of χ^2 equal to χ^2 divided by the number of measurements.

3.6. DISCUSSION

In comparison with our previously given values for ε, R_e, $q_{2,6}$ and $q_{2,12}$ (ref. 2d), the new results are based upon a much larger body of experimental data, especially due to the extension of the velocity range of NO from 600 to 2500 m/s. Moreover, to obtain the ε- and R_e-parameters independently, an absolute measurement of $\bar{\sigma}$ was performed.

The velocity averaging procedure of section 3.4.1 is much improved as compared to ref. 2d, resulting in a more pronounced damping. The angular resolution correction (section 3.4.3) takes the wobbling of the sixpole into account in a proper way, effectively reducing this correction to zero. In ref. 2d, neglecting the wobbling, this correction was assumed to amount to about 10% of A.

Finally, the results are now interpreted in s.a. including higher order terms, whereas in ref. 2d the authors employed only a linear approach.

In conclusion, the old parameter values must be regarded as obsolete.

Concerning the anisotropy parameters, especially the $q_{2,12}$-values (except for Ne) have changed to 0.7 instead of the old 0.4-value. The new result compares well to the value of $q_{2,12}$ for N_2-N_2 as discussed by Nyeland (ref. 23).

As before (see also refs. 2c and 2e), the $q_{2,6}$-parameter is found

to be considerably larger than the Unsöld value $(\alpha_\perp - \alpha_\parallel)/3\bar{\alpha} = 0.16$ (ref. 24). This difference is attributed to the much shorter probing distance of the present experiment as compared to the intermolecular distances where the Unsöld values become valid.

Objections could be raised against our simple potential model (Eq. (3.2)). Especially, our reasoning that old Legendre polynomials and terms of the form of Eq. (3.2) can be neglected may be criticized because we have included higher order terms in our theoretical treatment (s.a.). Actually, these higher order contributions become very large, at low velocities; in Table 3.3, the values in the last column are calculated using the linear approach (l.s.a.) of ref. 2d; for a more detailed comparison see ref. 11.

However, the higher order terms assume a substantial magnitude only there, where damping due to the velocity averaging is of paramount

N	A_g (s.a.) [%]	A_g (l.s.a.) [%]
1.25	2.0	2.1
1.75	1.9	2.5
2.25	1.8	3.4
2.75	1.7	3.7
3.25	1.6	4.5
3.75	1.5	5.8

Table 3.3. Comparison of sudden approximation (s.a.) and its linear approach (l.s.a.) at values for N, that correspond to anisotropic glory extrema. These calculations are performed for the parameters of NO-Ar of Table 3.1.

influence. Consequently, the fit values of $q_{2,12}-1.5q_{2,6}$ of Table 3.1 derive predominantly from the high velocity range where the arguments of section 3.3 are valid (see Table 3.3).

On the other hand, the damped average value at low velocities is well described by the non-glory contribution A_{ng}, which is properly derived using the linear approach (see ref. 12).

Application of s.a. to the system NO-Ne deserves a special justification because at the highest experimental velocities the non glory part (Eq. (3.18a)) of the anisotropy becomes debatable; as a matter of fact, those measurements reflect the behaviour of the system in the transition region where the attractive part of the potential loses its influence on the total collision cross section, in contrast to the employed Eq. (3.15a). Whether this point is responsible for the low values of $q_{2,12}$ (see Table 3.1, first row) shall be discussed in a forthcoming paper.

The present paper should be regarded as a presentation of mainly experimental material quantitatively interpreted using the very simple extended LJ 12-6 potential. We do not suggest that Eq. (3.2) together with the parameters of Table 3.1 can explain a broad spectrum of different properties. Certain shortcomings like the wrong assymptotic behaviour of the isotropic part at long distances shall be remedied, in the mentioned forthcoming paper where also an analysis shall be found as to where the intermolecular potential is sentively probed by the present measurements; this analysis permits, then, the use of an imperfect potential model for certain applications where the probing range coincides with ours.

REFERENCES

1a. J. Reuss, Scattering from oriented molecules in K.P. Lawley (Ed.), Molecular Scattering: Physical and chemical applications, Advances in Chemical Physics III, John Wiley, 1975, London

1b. H. Thuis, S. Stolte and J. Reuss, Comments on Atomic and Molecular Physics, Part D, Eds. Gordon and Breach, Science Publishers Inc., New York, to be published

2a. S. Stolte, thesis, Katholieke Universiteit, Nijmegen, 1972

2b. S. Stolte, J. Reuss and H.L. Schwartz, Physica 57 (1972) 254

2c. S. Stolte, J. Reuss and H.L. Schwartz, Physica 66 (1973) 211

2d. H.L. Schwartz, S. Stolte and J. Reuss, Chem.Phys. 2 (1973) 1

2e. H.P.M. Kessener and J. Reuss, Chem.Phys.Lett. 31 (1975) 212

3. G.C. Nielson, G.A. Parker and R.T. Pack, J.Chem.Phys. 66 (1977) 1396

4. J. Los, private communication

5. H. Beijerinck, private communication

6. D. Klaassen, Quarterly Report 53, Katholieke Universiteit, Nijmegen (1976) (The program is slightly modified.)

7. R.B. Bernstein and R.A. LaBudde, J.Chem.Phys. 58 (1973) 1105

8a. L. Zandee and J. Reuss, Chem.Phys. 26 (1977) 327

8b. L. Zandee and J. Reuss, Chem.Phys. 26 (1977) 345

8c. L. Zandee, J. Verberne and J. Reuss, Chem.Phys. 26 (1977) 1

9. E. Luzzatti, F. Pirani and F. Vecchiocattivi, Mol.Phys. 34 (1977) 1279

10. D. Poppe, Chem.Phys. 25 (1977) 29

11. D. Klaassen, H. Thuis, S. Stolte and J. Reuss, Chem.Phys. 27

(1977) 107

12. J.W. Kuijpers and J. Reuss, Chem.Phys. 4 (1974) 277

13. A.R. Edmonds, Angular Momentum in Quantum Mechanics, Princeton University Press, 1974, New Jersey

14. R. Düren and H. Pauli, Z.Phys.175 (1963) 227

15. S. Stolte and J. Reuss in R. Bernstein (Ed.), Atom-molecule collision theory: A guide for the experimentalist, Plenum, 1979, London

16. M. Jacobs and J. Reuss, Chem.Phys. 25 (1977) 425

17. P. Zugenmaier, Z.Angewan.Phys. 20 (1966) 184

18. S. Stolte, to be published

19. N.F. Verster, private communication

20. J. Hirschfelder, C. Curtiss and R. Bird, Molecular theory of gases and liquids, John Wiley, 1965, New York

21. T.M. Miller and B. Bederson, Advances in atomic and molecular physics, vol. 13, Academic Press, 1977, New York

22. K.T. Tang and J.P. Toennies, J.Chem.Phys. 66 (1977) 1496

23. C. Nyeland and G.D. Billing, Chem.Phys. 30 (1978) 401

24. N.J. Bridge and A.D. Buckingham, Proc.Roy.Soc. A295 (1966) 334

CHAPTER 4

THE ANGLE DEPENDENT MAITLAND-SMITH POTENTIAL FITTED TO TOTAL COLLISION CROSS SECTION MEASUREMENTS WITH AND WITHOUT m_j-STATE SELECTION, FOR NO-AR

4.1. INTRODUCTION

With state selection, total collision cross section measurements were performed in the velocity range 500 to 2500 m/s, for NO-inert gas systems (ref. 1). Recently, the measurements have been implemented by very accurate total cross section measurements without state selection, for NO-Ar in the range 800 to 3500 m/s. These measurements have been performed on the same machine where previously inert gas - inert gas systems were investigated (ref. 2). Thus, for NO-Ar we are in the unique position to dispose of three independent sources of information from which the intermolecular potential (IP) can be derived: the glories (and their quenching, a quadratic and higher order effect caused by the angle dependent part of the intermolecular potential (AIP)), the anisotropy of the total collision cross section A (mainly a first order effect caused by the AIP), and the absolute value of the total collision cross section; all data shall be analyzed concurrently in this chapter.

In ref. 1, a modified Lennard-Jones (LJ) 12-6 potential was employed to fit the anisotropy results. Although a good agreement was obtained this potential model suffers from intrinsic difficulties. Specifically, its invalid relation for the dispersion coefficient,

$C_6 = 2\,\varepsilon R_e^6$ should be replaced by $C_6 \simeq \varepsilon R_e^6$ (ref. 3), a feature that is nicely incorporated in the Maitland-Smith (MS) potential (ref. 4). Here ε and R_e stand for the depth and the position of the isotropic potential well.

An additional motivation to confront the combined experimental data of the present paper with predictions following from the MS potential stems from the fact that the inert gas measurements allowed a perfect fit with this model, whereas the LJ model had to be rejected (ref. 2c).

The analysis will be based on a truncated expansion of the potential into Legendre polynomials

$$V(R,\vartheta) = V_0(R) + V_1(R)P_1(\cos\vartheta) + V_2(R)P_2(\cos\vartheta) \qquad (4.1)$$

where R stands for the intermolecular distance; the angle ϑ is formed by the molecular axis (direction $\hat{r}_1$) and the vector between the centres of colliding partners (direction $\hat{R}$).

Unexpectedly, the inclusion of the second term of Eq. (4.1) proved to be of substantial influence on our effort to obtain a convincing fit for the combined experimental data.

Since we are not (yet) able to perform a real multiproperty analysis, a discussion is included of the range where the proposed potential is expected to be valid, i.e. of the probing distance.

As in ref. 1, we employed the Bernstein-Kramer sudden approximation (sa) for our analysis. A comparison with results in infinite order sudden approximation (IOS) is given in section 3.

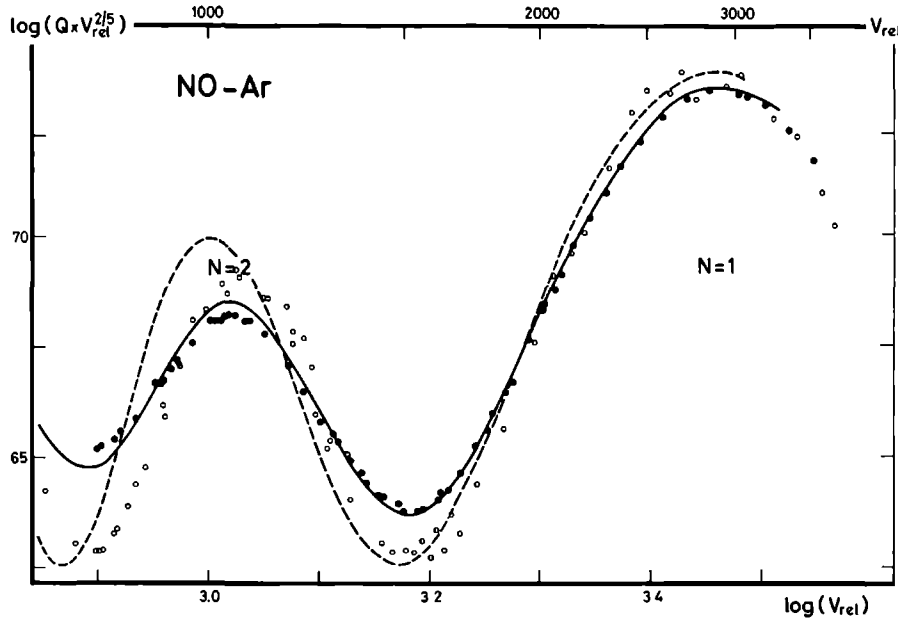

Fig. 4.1. For the system NO-Ar, the total collision cross section measurements (●) without state selection are fitted (solid line) in sa using the modified MS potential, see Table 4.1, with the parameters of Table 4.3. The dashed curve shows the calculated total cross section for the same ε and R_e value, omitting the angle dependent part of the potential (i.e. $q_{a,2} = q_{r,1} = q_{r,2} = 0$). The open circles (O) are the experimental values for the system Ar-Ar from ref. 2b to illustrate the presence of quenching, experimentally. The scattering of the measured points clearly demonstrates the progress in experimental accuracy.

4.2. THE TOTAL COLLISION CROSS SECTION DATA, WITHOUT STATE SELECTION

In Fig. 4.1. the glory structure of the total collision cross section for NO-Ar is displayed. The well defined scattering conditions of the crossed beam apparatus allow a direct deconvolution of the experimental data (ref. 2a, 2b); consequently, the result of Fig. 4.1 can be directly compared with theory.

Both beams are obtained from supersonic expansion, i.e. considerable rotational and electronical cooling of the NO-molecules occurs (ref. 1), resulting in a beam temperature $T_{\parallel}$ = 10-50 K. The lower $^2\Pi_{1/2}$-state is almost exclusively populated in contrast to the situation of ref. 1, where the $^2\Pi_{3/2}$-state was selected for the total cross section measurements. Concerning the rotational states, a mixture with $\langle j \rangle$ = 3/2 - 9/2 is present in the primary NO-beam, for the data of Fig. 4.1, whereas in ref. 1 the j = 3/2 state was selected. Higher j-values could lead to a significant influence of the terms of a multipole expansion, which are neglected in Eq. (4.1). Nevertheless, we have analyzed the data employing this equation because otherwise too many parameters would have to be introduced. Encouragingly, for the glory minima (N = 1.5) measurements were performed for $T_{\parallel}$ = 140 K and $T_{\parallel}$ = 10 K yielding the same total cross sections within 0.5% (the overall accuracy).

4.3. METHOD OF CALCULATION

4.3.1. FAILURE OF dwa AND lsa

In former investigations concerning the H_2-inert gas systems it was shown that a linear approximation (distorted wave approximation,

dwa) was adequate to describe the measured anisotropy of the total collision cross section A (ref. 5).

A linearized version of sa (lsa) has been shown to give results equivalent to dwa (ref. 6).

In the present case such an approach is doomed to fail; it does not predict any quenching of the non-state selected glories. From Fig. 4.1, however, it is clear that for NO-Ar significant quenching is present as compared to Ar-Ar. In the same figure, it is shown how the angle dependent terms of the MS potential adopted in this paper (see section 4) influence the glory behaviour.

Table 3 of ref. 1 demonstrates the necessity of including higher order terms (hots) when calculating the anisotropy A.

4.3.2. INFINITE ORDER SUDDEN APPROXIMATION vs. BERNSTEIN-KRAMER SUDDEN APPROXIMATION

The sudden approximation (sa) favoured by us is thoroughly discussed in ref. 7. Although the linearized version is not apt to describe the experiments (due to the large anisotropy of NO-Ar), for small anisotropies, however, it can be used to demonstrate the inadequacy of infinite order sudden (IOS) calculations which even yields the wrong sign for both the velocity averaged (non glory) contribution (chapter 5.6.2 of ref. 7) and the glory contribution (chapter 5.6.3 of ref. 7) to A. For the non state selected results the difference between non linear IOS and non linear sa is less devastating, see Fig. 4.2.

Also in this figure is shown (-----) the effect of an approximate application of the stationary phase method which is used in the deriva-

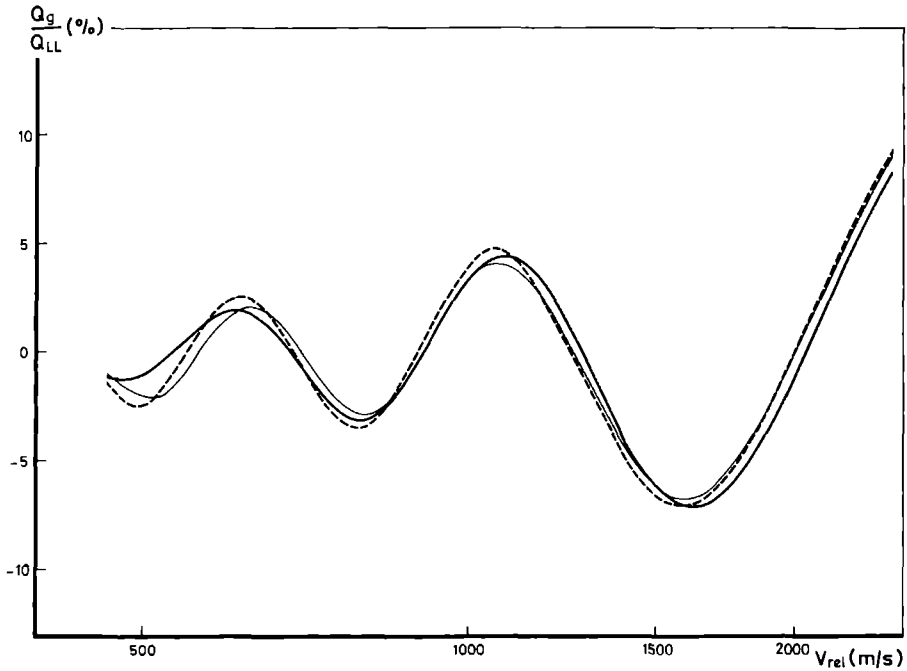

Fig. 4.2. Comparison of the total collision cross section calculated in IOS and sa, for the LJ 12-6 potential of Table 4.3 The glory cross section Q_g is given relative to the Landau Lifshitz cross section $Q_{LI} = 8.083(2\epsilon R_e^6/(\hbar v_{rel}))^{2/5}$. The curves ——— and ----- are obtained both in IOS, the latter one with an additional approximation concerning the angle dependent phase shift $\eta_1(\vartheta)$, a similar approximation (inducing small changes) is intrinsic for sa (———) presumably causing a comparable uncertainty.

tion of the sa-formulae of Table 4.1b. The RHS of the expression for $Q_g(\Theta_1,\phi_1)$ contains the angle dependent term $2\delta_m$, in the argument of the cosine, this term is proportional to the action integral $\int_{-\infty}^{+\infty} V'(t)dt$ taken along the glory trajectory (zero deflection angle), the glory trajectory is calculated solely from the TIP.

It is difficult (easy) to estimate the error introduced by this approximate determination of the action integral - neglected effect of AIP on glory phase shift - in sa (IOS) We assure that the deviations are very similar, for both methods. In IOS, then, we replace $\eta_1(\vartheta)$ by a parabola with its vertex $\eta_m(\delta)$ at $l = l_m(\vartheta)$ and a curvature determined by $\eta_m''(\vartheta)$, yielding curve (——). By numerical tests we have shown that the introduction of this approximation does lead to negligible deviations only. Next, we replace $l_m(\vartheta)/(|\eta_m''(\vartheta)|)^{1/2}$ by $l_{m,0}/(|\eta_{m,0}''|)^{1/2}$ (determined from the TIP, only) without introducing a serious error. Finally, $\eta_m(\vartheta)$ is replaced by $\eta_{l_{m,0}}(\vartheta)$ yielding curve (-----). This last step resembles the error introduced into sa by using an approximate value for the action integral. One observes a small shift of the extrema resulting in an effective overestimation of the product εR_e by about 2% in the experimental range of velocities. A change of amplitude is observed, too, leading to an underestimation of $q_{2,12}$ by about 5%. We must assume that in sa the same uncertainties are present.

There is little shift between IOS and sa (in case both employ the approximation discussed above), the amplitudes, however, are slightly different. Lacking further knowledge we base the following analysis on the sa amplitudes.

The formulae used in the different approximations were described in ref. 7 and are summarized in Table 4.1.

Table 4.1. Survey of used formulae.

In infinite order sudden approximation (IOS) the angle $\vartheta = \sphericalangle(\hat{R},\hat{r}_1)$ appears as a parameter (varying from 0 to π); for a fixed angle ϑ the phase shift $\eta(\vartheta)$ has to be calculated. Its maximum value $\eta_m(\vartheta)$ is assumed for the angular momentum quantum number $l_m(\vartheta)$; its second derivative is defined as $\eta''_m(\vartheta)$ for this value. The total collision cross section without (with) state selection requires the (weighted) average of $Q(\vartheta)$. G_s, proportional to $l_m(\vartheta)/(|\eta''_m(\vartheta)|)^{1/2}$ can be replaced by $G_s \sim l_{m,0}/(|\eta''_{m,0}|)^{1/2}$ (calculated from the IIP) without introducing a significant error.

In space fixed sudden approximation (sa) the angles $\Theta_1=\sphericalangle(\hat{r}_1,\hat{v}_{rel})$ and $\phi_1 - \phi$ (= azimuth of molecular axis around the asymptopic trajectories for $t \to -\infty$) are considered to be spacefixed during a collision. Phase shifts $\eta_{m,0}$ and related quantities are derived from the IIP. The integrand V' stands for the AIP; the $S^{(m)}$-integrals are defined in ref. 7. For the MS potentials numerical values for $l_{m,0}$, $\eta_{m,0}$, $\eta''_{m,0}$ and the $S^{(m)}$-integrals can be calculated from the series expansion in appendix B.

IOS: TOTAL COLLISION CROSS SECTION	
a) for 'molecule fixed angle' ϑ	$Q(\vartheta) = \frac{4\pi}{k^2} \Sigma\ (2l+1)\sin^2\eta_l(\vartheta)$ $= Q_{ng}(\vartheta) + Q_g(\vartheta)$ with $Q_{ng}(\vartheta) = F_s[1 + \frac{2}{s-1} q_{2,s} P_2(\cos\vartheta)]$ and $Q_g(\vartheta) = G_s \cos[2\eta_m(\vartheta) - \frac{\pi}{4}]$
b) with state selection	$Q_{sts} = \langle jm_j \vert Q(\vartheta) \vert jm_j \rangle$ with $\vert jm_j\rangle$ function of θ_1, ϕ_1 and $\vartheta = \theta_1$
c) without state selection	$Q = \frac{1}{2j+1} \Sigma_{m_j} Q_{sts}$ $= F_s + \frac{1}{2} G_s \int_{-1}^{+1} \cos[2\eta_m(\vartheta) - \frac{\pi}{4}] d(\cos\theta_1)$
	$F_s = 2\pi \left[2 f_s \frac{C_s}{\hbar v}\right]^{2/(s-1)} \Gamma(\frac{s-3}{s-1}) \sin(\frac{\pi}{2} \frac{s-3}{s-1})$ $G_s = -\frac{4\pi l_{m,0}}{k^2} \sqrt{\frac{\pi}{\lvert\eta''_{m,0}\rvert}}$ $f_s = \frac{\pi^{1/2}}{2} \Gamma(\frac{s-1}{2}) / \Gamma(s/2)$

Table 4.1a.

sa: TOTAL COLLISION CROSS SECTION	
a) for 'space fixed angles' Θ_1, ϕ_1	$Q(\Theta_1,\phi_1) = Q_{ng}(\Theta_1,\phi_1) + Q_g(\Theta_1,\phi_1)$ with $Q_{ng}(\Theta_1,\phi_1) = F_s[1 - \frac{s-3}{s(s-1)} q_{2,s} P_2(\cos\Theta_1)]$ and $Q_g(\Theta_1,\phi_1) = G_s \cos[2\eta_{m,0} - \frac{\pi}{4} - 2\delta_m(\Theta_1,\phi_1-\phi)]$
b) with state selection	$Q_{sts} = \langle jm_j \vert Q(\Theta_1,\phi_1) \vert jm_j \rangle$
c) without state selection	$Q = \frac{1}{2j+1} \sum_{m_j} Q_{sts}$ $= F_s + \frac{1}{4\pi} G_s \int_0^{2\pi} d(\phi_1-\phi) \int_{-1}^{+1} d(\cos\Theta_1)$ $\cos[2\eta_{m,0} - \frac{\pi}{4} - 2\delta_m(\Theta_1,\phi_1-\phi)]$
	$2\delta_m = + \frac{1}{\hbar} \int_{-\infty}^{\infty} V'(t)dt =$ $\frac{k\varepsilon R_c}{\hbar v_{rel}} \{-\frac{1}{2} q_{2,r} S^{(m)}(r,0,0) + \frac{1}{2} q_{2,a} S^{(m)}(a,0,0)$ $+ \frac{3}{2} \cos^2\Theta_1 [q_{2,r} S^{(m)}(r,2,0) - q_{2,a} S^{(m)}(a,2,0)]$ $+ \frac{3}{2} \sin^2\Theta_1 \cos^2(\phi_1-\phi) [q_{2,r} S^{(m)}(r,0,2)$ $- q_{2,a} S^{(m)}(a,0,2)] - \sin\Theta_1 q_{1,r} S^{(m)}(r,0,1)\}$

Table 4.1b.

The NO molecule possesses a half filled π-orbital; consequently, in collision with inert gas atoms two potential surfaces are present, V_+ and V_- (ref. 8). In the following, we shall treat the system by a single potential surface, however, as Nielson *et al.* (ref. 8) have argued that the difference V_d $(V_+ - V_-)/2$ is very small in comparison to the average potential $V_a = (V_+ + V_-)/2$.

The angle dependence is incorporated by the use of the truncated Legendre expansion (Eq. (4.1). Higher order Legendre polynomials (*holps*, to be distinguished from *hots*) are neglected; concerning the analysis of A this was discussed in ref. 1; $V_n(R)$ terms with $n > 2$ influence A_g through hots. Although it was argued (ref. 1) that inclusion of these hots is necessary (failure of linearized theory, see section 4.3) the main contribution to A_g originates from linear terms, except at low velocities, but there massive damping of the glory structure due to velocity averaging renders A_g rather unimportant for the analysis.

On the other hand, the new results on quenched glories with non state selected beams are entirely caused by quadratic and higher order terms. Here it is difficult to judge to what extend $V_n(R)$-terms with $n > 2$ (appearing as factors of holps) are of influence. According to ref. 8 at least a strong repulsive V_3-term is present, too. Neglecting this term produces an effective V_1-term, that includes some of the V_3-effects.

For the V_1-term we only consider a repulsive part. Actually, the excentricity of the NO-molecule causes a centre of mass shift necessitating a transformation whereby a V_1-term originates from the V_0-term

	POTENTIALS
General form	$V(R,\vartheta) = V_0(R) + V_1(R)P_1(\cos\vartheta) + V_2(R)P_2(\cos\vartheta)$
Lennard Jones	$V_0(R) = \varepsilon\{(R_e/R)^{12} - 2(R_e/R)^6\}$ $V_1(R) = 0$ $V_2(R) = \varepsilon\{q_{2,12}(R_e/R)^{12} - 2q_{2,6}(R_e/R)^6\}$
Maitland-Smith ref. 4	$V_0(R) = \varepsilon\{(6/(n-6))(R_e/R)^n - (n/(n-6))(R_e/R)^6\}$ $V_1(R) = \varepsilon q_{1,r}(6/(n-6))(R_e/R)^n$ $V_2(R) = \varepsilon\{q_{2,r}(6/(n-6))(R_e/R)^n - q_{2,a}(n/(n-6))(R_e/R)^6\}$ with $n = 13 + \gamma(R/R_e-1)$; $\gamma = 9$, 10.
non glory range	$V_1(R) = 0$; $V_2(R) = q_{2,a}V_0(R)$; $V_0(R) = -(1.70\pm.06)(R/R_e)^{6.35\pm.07}$
Nielson et al. for NO-Ar ref. 8	$V_n(R) = V_n^{SCF}(R) + V_n^{COR}(R)$, with $V_0^{SCF}(R) = 9.953 \times 10^{-17} \exp(-0.47679\ R - 0.022871\ R^2)$ $V_0^{COR}(R) = -B_{01} \exp(-0.40513\ R - 0.007262\ R^2)$, $R \leq 2.997$ Å $= -C_6(0)\ R^{-6} - (B_{01} - 0.00496\ C_6(0))$ $\exp(-0.40513\ R - 0.00726\ R^2)$, $R \geq 2.997$ Å $V_1^{SCF}(R) = -3.5805 \times 10^{-21} \exp(+0.2486\ R - 0.044058\ R^2)$ $V_1^{COR}(R) = -2.0769 \times 10^{-20} \exp(-0.093604\ R - 0.014404\ R^2)$ $V_2^{SCF}(R) = 8.3480 \times 10^{-17} \exp(-0.44913\ R - 0.02249\ R^2)$ $V_2^{COR}(R) = -B_{21} \exp(-0.37746\ R - 0.0080123\ R^2)$, $R \leq 3.045$ Å $= -C_6(2)\ R^{-6} - (B_{21} - 0.004264\ C_6(2))$ $\exp(-0.37746\ R - 0.0080123\ R^2)$, $R \geq 3.045$ Å

Table 4.2. The three analyzed potentials (LJ, MS and NPP) are summarized. The parameters ε and R_e stand for the well depth and its position. All potentials are series expansions in Legendre polynomials P_n. The anisotropic parameters $q_{\lambda,n}$ determine the strength of the AIP. For the NPP potential numerical values are shown (see ref. 8) except for the parameters, that were adapted to fit the experimental data ($C_6(0) = 85 \times 10^{-19}$ J Å^6, $C_6(2)/C_6(0) = 0.2$, $B_{01} = 3.24 \times 10^{-21}$ J, $B_{21} = 1.85 \times 10^{-21}$ J).

also at long distances. However, as this excentricity is extremely small we neglect an attractive contribution to V_1.

Responsible for the repulsive V_1-term is the bulge of the electron cloud outwards of the N-atom which has the smaller nuclear charge.

Now we have to choose a potential model. The angle dependent LJ 12-6 potential (see Table 4.2) has the comfortable property of only two adjustable parameters for the isotropic part (IIP), i.e. ε and R_e, and two parameters for the AIP, i.e. $q_{2,6}$ and $q_{2,12}$. A nearly perfect fit to the measurements of A has been reported (ref. 1). In section 4.1, we already have indicated an intrinsic shortcoming of this model (ref. 3). The unrealistic form of this potential causes, too, the impossibility to obtain a reasonable fit to the non state selected glory measurements of Fig. 4.1.

In Table 4.2. the angle dependent MS potential is defined, too. It contains three parameters for the IIP, i.e. ε, R_e and γ. The parameter γ is fixed to 9 or 10 on the basis of experience with pure inert gas systems (ref. 2). For Ar-Ar the deviations are small between the MS

potential and the BFW potential (Barker, Fisher, Watts (ref. 9)), the latter one resulting from an extensive multiproperty analysis.

The ATP is chosen in a rather arbitrary way (see Table 4.2), that contains hopefully enough flexibility to describe a large set of different experiments.

For $1.5 < R/R_e < 2$ the MS potential can be approximated by inverse power expressions (see Table 4.2). We have used the corresponding entries of this table to calculate the non glory contribution to A and the glory averaged total collision cross section. The exponent s and the coefficient D_s were derived by putting $D_s(R_e/R)^s = n(n-6)^{-1}(R_e/R)^6$ and fitting the derivatives of both expressions, too, at distances $(1.5 - 2)R_e$. In Table 4.2 the uncertainties originate from the range of distances considered.

The use of the inverse power expression was tested by Landau-Lifshitz-like approximation, concerning the glory averaged cross section (agreement within 0.5% was found). By a dwa calculation A_{ng} was tested (agreement within 3%).

A theoretical potential for NO-Ar has been derived by Nielson et al. (ref. 8) using the electron gas model developed by Gaydaenko and Nikulin and Gordon and Kim (ref. 10). The form of this potential can also be found in Table 4.2. The parameters B_{01}, $C_6(0)$, $C_6(2)$ and B_{02} are fitted to the observed glory phase, the measured absolute value of the total collision cross section, the non glory anisotropy and the glory amplitude of A for the lowest observed glory number $N = 1\frac{1}{4}$, respectively. These fit calculations were done in (linear) dwa. At $N = 1\frac{1}{4}$ quenching effects are of minor influence. The V_1-term of ref. 8 is not considered; this term only causes quenching effects which we are not

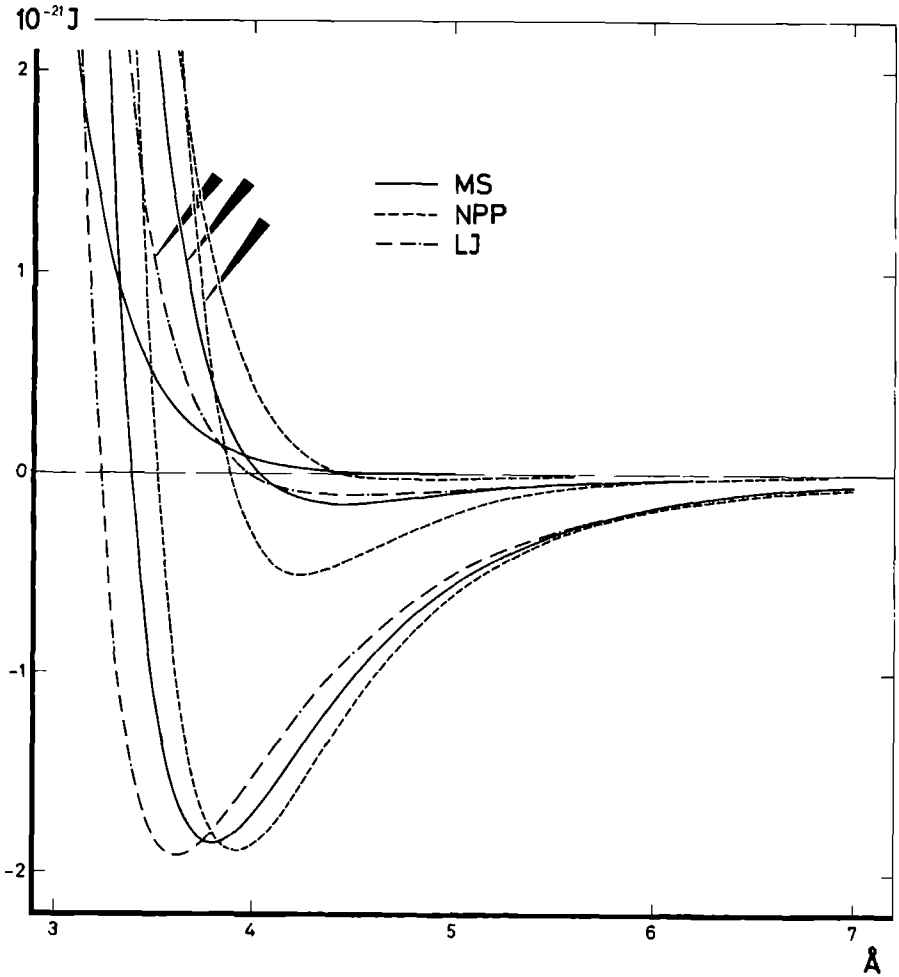

Fig. 4.3. The best Maitland-Smith potential (MS) compared to the Lennard-Jones 12-6 potential (LJ) of ref. 1 and to the adapted theoretical potential (NPP) of Nielson et al. (ref. 8). The deep (shallow, with arrows) curves correspond to V_0 (V_2); the two remaining curves to V_1. The arrows indicate the position ($R/R_e \approx 0.96$) where V_2 is probed; the probed relative values V_2 (0.96 R_e) lie satisfyingly close. Moreover, the non glory probed values V_2 ($R \approx 1.8\ R_e$) show good agreement.

able to treat in dwa. Calculations in sa were not performed because of the rather large computational effort required.

All potentials of Table 4.2 are displayed in Fig. 4.3.

4.5. RESULTS AND DISCUSSION

A complete analysis can only be performed for the system NO-Ar where the total collision cross section with and without state selection has been measured (see Figs. 4.1 and 4.4).

In Table 4.3 the results are summarized for the potentials discussed in the previous section. Entries for the LJ potential are those of ref. 1, which should be regarded as obsolete due to the fact that the new measurements of Fig. 4.1 can be poorly described by this model.

	ε [10^{-21} J]	R_e [Å]	C_6 [10^{-19} J Å^6]	$q_{2,a}$	$q_{1,r}$	$q_{2,r}$
LJ	1.91(3)	3.62(6)	85	0.20(2)	-	0.70(4)
MS	1.85(3)	3.86(6)	61	0.20(2)	0.10(2)	0.75(4)
NPP	1.9	3.9	85	0.20(2)	*	*
Theory	1.45	4.0	66	0.14	*	≥ 1

Table 4.3. Results for NO-Ar. The NPP is calculated with the original B_{01}, B_{21}, $C_6(0)$ and $C_6(2)$ multiplied by 3, 3.5, 1.3 and 1.8, see Table 4.2. The theoretical values are taker from ref. 8. For comparison $q_{2,a} \sim (\alpha_{\parallel} - \alpha_{\perp})3\bar{\alpha} = 0.16$, α stands for the polarizability. In this table * means that the corresponding parameter cannot be defined.

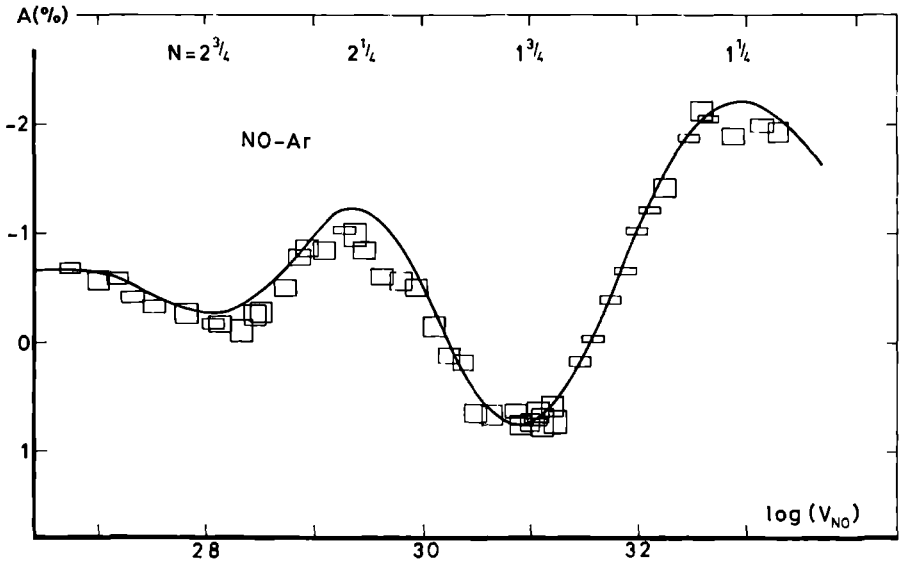

Fig. 4.4. The anisotropy A vs. the primary velocity V_{NO}. The squares indicate the uncertainty in the velocity determination (3%); in vertical direction they display the statistical error in A. On the top the glory numbers N are shown. The curve corresponds to the best fit with the MS potential (Table 4.3).

On the other hand, the NPP potential has not been used in conjunction with sa; however, linear theory was employed where we expect it to be valid, i.e. at high velocities; quenching effects have not been investigated with the NPP potential. Although the NPP potential is the only theoretical potential available, its accuracy should not be overestimated. First of all, the well depth is too shallow by about a factor 1.7. We have partially remedied this shortcoming by introducing an effective $C_6(0)$-constant of 1.3 times the theoretical value of ref.

8. In this way, the absolute value of the total cross section was brought into agreement with experiment. Similarly, the theoretical $q_{2,a}$ ($= C_6(2)/C_6(0)$) was increased by a factor 1.4, in order to obtain a fit to the non glory anisotropy A_{ng}. Spurred by a private communication from R.T. Pack we have considered the pre-exponential factors of the correlation term (B_{01} and B_{21}) as free parameters; fitting our results the value of B_{01} had to be increased by a factor 3 in order to obtain agreement with the phase of the glory undulation and the value of B_{21} by a factor 3.5 to obtain the proper amplitude of A. The resulting NPP-potential is displayed in Fig. 4.4; contriving its final form we were forced to take certain liberties, which surpass the limits originally intended by the authors of ref. 8, especially what concerns the $C_6(0)$ and $C_6(2)$ value. To our defence we might argue that the use of the electron gas model for a system possessing an unfilled electron shell can introduce unforeseen errors so that the form of the NPP potential is not quite correct and therefore necessitates the adaptions performed by us.

The most extensive analysis was performed using the MS potential. Here quenching phenomena were treated, too.

The ϵ and R_e values of Table 4.3 are different for the LJ and MS potential. As the MS potential has a "C_6-constant" decreasing with increasing R, the same ϵR_e^6 values would lead to an about 14% smaller total collision cross section for MS as compared to LJ.

The MS long range C_6 constant ($\epsilon R_e^6 = 6.12 \times 10^{-18}$ J Å^6) has been found from a fit to the absolute value of the total cross section (ref. 1) and differs satisfyingly by less than 10% from the theoretical (original) value 6.60×10^{-18} J Å^6 (ref. 8). (It should be emphasized,

however, that the analytical form of the MS model was mainly chosen to reproduce the IIP at "real" distances and not at its asymptotic range.)

The product $\varepsilon R_e = 7.14 \times 10^{-21}$ J Å mainly describes the phase of the glory phenomena. The total collision cross section (Fig. 4.1) was measured with an estimated accuracy of the absolute value of the velocity of about 0.5%, whereas the measurements of Fig. 4.4 were performed with a corresponding accuracy of about 2.5%. The latter results yield a product εR_e of about 3% lower than the former results. We adopted the more recent and accurate information of Fig. 4.1, keeping in mind, however, that εR_e is overestimated by about 2% due to the use of the approximation discussed in section 3.3.2.

The anisotropy in the attractive part of the potential is described by the parameter $q_{2,a}$ whose value is derived from the determination of A_{ng}. The value for the MS potential has an estimated accuracy of $\pm$10%. The uncertainty introduced by the method of calculation (section 3) is much smaller. Whereas the long range behaviour of V_0 is reproduced within 10%, the MS potential results in a long range value for V_2 that differs by about 30% from the theoretical value ($q_{2,a} = 0.14$, ref. 9).

New as compared to our earlier interpretation is the recognition that a substantial V_1-term has to be included in the analysis to permit a proper description of the glory quenching result. Formerly, we had disregarded this term arguing that the very small excentricity of NO would lead to negligible effects. However, in the repulsive part of the potential the difference of extension of the electron cloud for the N- and O-side of the molecule must appear (see also ref. 8). We were able to fit the results with $q_{1,r} = 0.10 \pm 0.02$ and $q_{2,r} = 0.75 \pm 0.04$. This latter value and its uncertainty does not include the underestimation

by 5% due to the use of the approximation discussed in section 4.3.2. Both parameters are derived from the quenched isotropic glory of Fig. 4.1 and the anisotropic glory of Fig. 4.4; $q_{1,r}$ must be regarded as an effective value including contribution from a neglected V_3-term. On the other hand $q_{2,r}$ includes only small effects of neglected higher order terms (e.g. with V_3 and V_4) which enter the results only through non-linear approximations.

The largest discrepancy between theory and experiment concerns the value of $q_{2,r}$. Nielson et al. show that for 2 Å $\leq$ R $\leq$ 3.5 Å the ratio V_2/V_0 varies from 1.06 to 1.30. This is the quantity which the electron gas model (used in ref. 8) gives most accurately. Perhaps the discrepancy points out again the intrinsic difficulty of that model when applied to systems with unfilled electron shells.

For NO-Kr, -Xe measurements of the total collision cross section without state selection are lacking, therefore an independent fit of $q_{1,r}$ is impossible. If we assume $q_{1,r} = 0.1$ as in the case of NO-Ar, we find for the MS potential parameters $\varepsilon(Kr) = 2.15 \times 10^{-21}$ J, $R_e(Kr) = 3.93$ Å, $\varepsilon(Xe) = 2.80 \times 10^{-21}$ J, $R_e(Xe) = 4.14$ Å, $q_{2,r}(Kr,Xe) = 0.75 \pm 0.03$ and $q_{2,a}(Kr,Xe) = 0.20 \pm 0.02$.

In ref. 11, Olson and Bernstein have shown how to estimate anisotropy parameters from glory quenching for the system Li-NO, utilizing an LJ potential. One finds for $q_{2,a} = 0.20$ and $q_{1,r} = 0$ the value $q_{2,r} = 0.72$ and for $q_{2,a} = 0.20$ and $q_{1,r} = 0.10$ the value $q_{2,r} = 0.69$.

The validity of the potential derived (Tables 4.1 and 4.2) is restricted. The anisotropy measurements probe distances of $R \approx 0.96\ R_e$, concerning A_g, $1.4\ R_e < R < 2.6 R_e$ is probed by A_{ng}, see Appendix C. Whereas the probing distances of A_g are rather velocity independent,

a significant shift to larger R values takes place for low velocities if one considers the distances probed by A_{ng}.

It is satisfying that the three (concerning their mathematical form very different) potential models displayed in Fig. 4.3 agree rather well with each other especially where sensitive probing occurs by the here described experiment.

1. H. Thuis, S. Stolte and J. Reuss, accepted for publication in Chem.Phys.

2a. C.A. Linse, J.J.H. van den Biesen, E.H. van Veen, C.J.N. van den Meijdenberg and J.J.M. Beenakker, to be published in Physica

2b. C.A. Linse, J.J.H. van den Biesen, E.H. van Veen and C.J.N. van den Meijdenberg, to be published in Physica

2c. J.J.H. van den Biesen, F.A. Stokvis, F.H. van Veen and C.J.N. van den Meijdenberg, to be published in Physica

3. K.T. Tang and J.P. Toennies, J.Chem.Phys. 66 (1977) 1496

4. C.C. Maitland and E.B. Smith, Chem.Phys.Lett. 22 (1973) 443

5a. L. Zandee and J. Reuss, Chem.Phys. 26 (1977) 327

5b. L. Zandee and J. Reuss, Chem.Phys. 26 (1977) 345

6. D. Klaassen, H. Thuis, S. Stolte and J. Reuss, Chem.Phys. 27 (1977) 107

7. S. Stolte and J. Reuss in Atom-molecule collision theory A guide for the experimentalist, R.B. Bernstein, ed., Plenum Press, New York (1979)

8. G.C. Nielson, G.A. Parker and R.T. Pack, J.Chem.Phys. 66 (1977) 1396

9. J.A. Barker, R.A. Fisher and R.O. Watts, Mol.Phys. 21 (1971) 657

10a. V.I. Gaydaenko and V.K. Nikulin, Chem.Phys.Lett. 7 (1970) 360, V.K. Nikulin, Zh.Tekh.Fiz. 41 (1971) 41

10b. R.G. Gordon and Y.S. Kim, J.Chem.Phys. 56 (1972) 3122, Y.S. Kim and R.G. Gordon, J.Chem.Phys. 60 (1974) 1842

11. R.F. Olson and R.B. Bernstein, J.Chem.Phys 50 (1969) 216

The investigations described in this thesis certainly are not the final answer to all questions that can be raised about the anisotropic part of the potential for NO-inert gas systems. In any case, the success of piecing together the results of several complementary experimental methods may be an encouragement to perform similar epxeriments concerning the determination of the total collision cross section without state selection for the systems NO-Kr, -Xe, and -Ne. However, conclusive information of the AIP can be expected only from a much more extensive multiproperty analysis. The case of NO-Ne must be further investigated because of its interesting and different features.

The experiment presently performed by the Leiden group concerning O_2-Ar will contribute to further knowledge; the absence of odd terms of the Legendre polynomial expansion will facilitate the analysis. State selection with inhomogeneous magnetic fields looks promising for O_2 so that also in this case the full wealth of experimental information may be at the disposal of those who want to determine the AIP for O_2-inert gas systems.

It is possible to apply the method of state selection and preferential orientation to other dipole molecules in their ground state (for instance NH_3, N_2O and O_3) or even to metastable $H_2^\dagger$ and $CO^\dagger$ with their presumably much larger anisotropy. NH_3 is very interesting because of the possibility to investigate special steric features of the hydrogen bridge, for instance in a collision with methane.

From a chemists point of view state selection is very important. For instance steric factors and internal energy dependence of the

chemiluminescent reactions $N_2O + Ba \rightarrow BaO + N_2^{\dagger}$ and $O_3 + NO \rightarrow O_2 + NO_2^{\dagger}$ are under investigation. Other reactions are accessible by laser fluorescence methods. State-to-state reactions contain the promise of real understanding of what is actually going on in chemistry.

A1. THE MEASURED INTENSITIES AND THE EXPERIMENTAL ANISOTROPY A^e

The experimental method is essentially the same as described in ref. 1, however, the role of the Rabi-deflection magnet is taken over by the wobbling of the sixpole. This wobbling also replaces the beam chopper, needed for phase-sensitive detection.

The four different intensities (Table A.1) measured during the experiment are inserted in the following relations

$$I_3 = I_1 \exp[-\frac{v_{NO}}{v_{rel}} nl\sigma_{\parallel}^e], \quad \text{and} \quad I_4 = I_2 \exp[-\frac{v_{NO}}{v_{rel}} nl\sigma_{\perp}^e] \qquad (A.1)$$

The experimental anisotropy A^e is extracted from these relations, yielding

$$A^e \equiv \frac{\sigma_{\parallel}^e - \sigma_{\perp}^e}{\sigma_{\parallel}^e} = [\ln(\frac{I_4}{I_3}) - \ln(\frac{I_2}{I_1})]/\ln(\frac{I_1}{I_3}) \qquad (A.2)$$

where $\sigma_{\parallel}^e$ and $\sigma_{\perp}^e$ stand for the experimental cross sections for the two orientations of the quantization axis, v_{NO} and v_{rel} for the primary beam velocity and the relative velocity between the colliding molecules. The density of the target molecules and the length of the scattering region are denoted by n and l.

Intensity	Secondary beam	Direction of magnetic field
I_1 (I_3)	off (on)	$\parallel$
I_2 (I_4)	off (on)	$\perp$

Table A.1.

A2. SEQUENCE OF MEASURING AND STATISTICS

To determine A^e, the four intensities are repeatedly measured in such an order that linear drift instabilities in the beam and random fluctuations are compensated for and averaged out. Each intensity is measured for 20 seconds with an accuracy of about 4×10^{-4}. A complete cycle consists of four blocks $T_1 \ldots T_4$ each of 24 intensities, 12 with $\hat{B}.\hat{v}_{rel} = 1$ ($\parallel$) and 12 with $\hat{B}.\hat{v}_{rel} = 0$ ($\perp$). For instance $T_1(T_2)$ and $T_3(T_4)$ are periods where the secondary beam is off (on). In order to avoid systematic sequential errors T_1 and T_2 both start with the magnetic field in the parallel and T_3 and T_4 in perpendicular direction.

The total of data to produce one value of A^e consists of 30-40 blocks. The individual value for $D_i = (I_1 - I_2)/I_1$ ($i = 1, 3$) are calculated from the first or third period (T_1 or T_3). The average $\langle D_i \rangle$ is expected to be zero, as it measures the anisotropy in the unscattered beam. Similarly, quantities $D_j = (I_3 - I_4)/I_3$ ($j = 2, 4$) are formed from the intensities of blocks T_2 and T_4. Their average values $\langle D_2 \rangle$ and $\langle D_4 \rangle$ contain the anisotropy; their standard deviations are ΔD_2 and ΔD_4.

The denominator of Eq. (A.2) contains the attenuation $N = I_1/I_3$

which is chosen such that $\ln N \approx 1$. The intensities I_1 are taken from all T_1 or T_3 periods, I_3 from all T_2 or T_4 periods. The average value is given by $\langle N_{iJ} \rangle = \langle I_1 \rangle_i / \langle I_3 \rangle_J$ with $i,J = 1, 2$ or $3, 4$, respectively. All values of D_J that lie outside three times the standard deviation from the average $\langle D_J \rangle$ are excluded.

From $\langle D_i \rangle$, $\langle D_J \rangle$ and $\langle N_{iJ} \rangle$ we obtain the values of A^e and its standard deviation S. With the data of T_1 and T_2 periods we can form (using $I_1 - I_2 \ll I_1$ and $I_3 - I_4 \ll I_3$)

$$A^e_{1,2} = \frac{\ln[1 + \langle D_1 \rangle - \langle D_2 \rangle]}{\ln \langle N_{12} \rangle} \quad ; \quad S_{1,2} = \frac{(\Delta D_1)^2 + (\Delta D_2)^2}{\ln \langle N_{12} \rangle} \qquad \text{(A.3a)}$$

and with T_3 and T_4

$$A^e_{3,4} = \frac{\ln[1 + \langle D_3 \rangle - \langle D_4 \rangle]}{\ln \langle N_{34} \rangle} \quad , \quad S_{3,4} = \frac{(\Delta D_3)^2 + (\Delta D_4)^2}{\ln \langle N_{34} \rangle} \qquad \text{(A.3b)}$$

In practice the values of $A^e_{1,2}$, $S_{1,2}$ and $A^e_{3,4}$, $S_{3,4}$ are equal, so we obtain as final result

$$A^e = \tfrac{1}{2}[A^e_{1,2} + A^e_{3,4}] \quad \text{and} \quad S = \frac{S_{1,2} S_{3,4}}{2}$$

REFERENCE

1. S. Stolte, thesis, Katholieke Universiteit, Nijmegen, The Netherlands, 1972

Table A.2 - A.5. Survey of the experimental data on the anisotropy. The first column contains the numbers of the paper tapes that bear all the information of one measurement of the anisotropy; the second column, the most probable NO velocity tuned by the velocity selector; the third column, the weighted average of the relative velocity; the last column, the anisotropy and its statistical error.

Table A.2. NO-Ne

Tape no.	v_{NO} [m/s]	$\langle v_{rel} \rangle$ [m/s]	A(exp) [‰]
423	457	492	-0.90 ± 0.73
466	480	514	+0.58 ± 0.54
465	503	535	-0.28 ± 1.60
467	503	535	-0.27 ± 0.35
464	548	578	+1.00 ± 0.57
468	594	622	+0.90 ± 0.80
469	651	677	-2.09 ± 1.10
476	679	704	+0.50 ± 0.80
477	679	704	+0.58 ± 0.59
422	686	711	-1.20 ± 1.05
417	777	799	-14.90 ± 0.58
426	850	871	-17.22 ± 1.33
418	914	934	-13.32 ± 0.92
419	960	979	-12.35 ± 1.20
420	1143	1160	-7.72 ± 1.70
567	1312	1328	-0.67 ± 0.49
568	1408	1423	+0.92 ± 0.89
562	1499	1514	+0.45 ± 1.70
563	1884	1897	+5.81 ± 1.40
564	2048	2061	+2.58 ± 0.71
565	2211	2224	+3.06 ± 1.01
566	2375	2388	+2.03 ± 2.30

Table A.3. NO-Ar

Tape no.	v_{NO} [m/s]	$\langle v_{rel} \rangle$ [m/s]	A(exp) [°/oc]
146	432	507	-7.62 ± 0.50
142/143/ 150/151	476	546	-6.65 ± 0.52
147	499	567	-5.33 ± 0.82
149	520	585	-5.55 ± 0.53
141	540	603	-3.90 ± 0.36
152	566	626	-2.86 ± 0.35
144	604	661	-2.55 ± 0.38
283	642	696	-0.95 ± 1.10
145/290	647	702	-1.45 ± 0.44
291	678	730	-0.97 ± 0.96
292	700	751	-2.41 ± 0.90
295	710	760	-2.58 ± 0.74
293	748	796	-4.83 ± 0.72
294	770	817	-7.59 ± 0.78
305/435	777	824	-8.32 ± 0.64
304	812	857	-8.14 ± 0.79
303/427/ 428/429/ 431/432	845	889	-10.13 ± 0.32
436	868	911	-9.72 ± 1.20
352	879		-8.31 ± 0.72
319/354	914	956	-5.98 ± 0.52

Table A.3 (continued)

Tape no.	v_{NO} [m/s]	$\langle v_{rel} \rangle$ [m/s]	A(exp) [$^{o}/_{oo}$]
326	947	987	-5.53 ± 0.87
320	980	1020	-4.94 ± 0.87
324	1014	1053	-1.53 ± 0.79
321	1048	1086	+1.27 ± 0.88
325	1080	1117	+1.95 ± 0.79
356	1113	1149	+6.73 ± 0.85
357	1152	1187	+6.72 ± 0.84
362	1216	1250	+6.56 ± 0.78
384	1222	1256	+7.68 ± 0.88
363	1250	1284	+7.53 ± 0.91
517	1261	1295	+7.34 ± 0.33
385	1269	1303	+6.62 ± 1.00
364	1284	1317	+7.55 ± 1.24
386	1316	1349	+5.99 ± 1.00
519	1392	1424	+1.84 ± 0.35
518	1435	1466	-0.27 ± 0.42
523	1479	1510	-3.82 ± 0.27
524	1523	1553	-6.45 ± 0.34
520	1566	1596	-10.06 ± 0.36
525	1610	1640	-12.05 ± 0.34
522	1653	1682	-14.12 ± 0.80
521	1740	1769	-18.60 ± 0.34
554	1781	1809	-21.20 ± 0.96

Table A.3 (continued)

Tape no.	v_{NO} [m/s]	$\langle v_{rel} \rangle$ [m/s]	A(exp) [‰]
534	1827	1855	-20.46 ± 0.41
535	1914	1942	-18.99 ± 0.76
546	2044	2072	-19.80 ± 0.56
555	2115	2143	-19.40 ± 0.87

Table A.4. NO-Kr

Tape no.	v_{NO} [m/s]	$\langle v_{rel} \rangle$ [m/s]	A(exp) [‰]
116/117	430	468	-7.81 ± 0.37
114/115	475	510	-5.85 ± 0.29
127	494	528	-5.25 ± 0.41
112/113/ 122/123/ 124	520	552	-4.44 ± 0.19
126	540	571	-4.82 ± 0.39
110/111	560	590	-5.96 ± 0.28
125	582	611	-6.67 ± 0.27
118/119/ 120	604	632	-8.00 ± 0.18
287	642	669	-7.22 ± 0.89
288	653	679	-6.80 ± 0.80
311	670	696	-4.87 ± 0.89
255/259	675	701	-4.92 ± 0.80
296/286	711	736	-1.84 ± 0.59
297/370	744	768	-1.47 ± 0.63
380	758	781	-1.90 ± 1.07
371	779	801	+0.89 ± 0.78
264	787	810	+1.57 ± 0.86
308	812	830	+0.95 ± 0.81
309	845	866	-0.66 ± 0.95
371	879	900	+0.44 ± 0.81

Table A.4 (continued)

Tape no.	v_{NO} [m/s]	$\langle v_{rel} \rangle$ [m/s]	A(exp) [‰]
369/370/ 318/404	912	932	-3.58 ± 0.40
316	982	1001	-10.77 ± 0.90
347/405	1014	1033	-12.41 ± 0.43
317/407	1049	1067	-13.46 ± 0.60
406	1097	1115	-15.22 ± 0.51
322	1113	1131	-14.64 ± 0.88
408	1142	1159	-14.65 ± 0.72
345	1152	1169	-11.17 ± 0.76
375	1175	1192	-9.17 ± 0.81
409/346/ 387	1186	1203	-10.06 ± 0.43
360	1222	1239	-8.27 ± 0.82
388	1234	1250	-8.18 ± 1.01
389	1280	1296	-3.42 ± 1.10
391	1325	1341	+0.50 ± 0.85
392	1371	1387	+4.70 ± 0.95
529	1392	1407	+4.75 ± 0.34
528	1436	1451	+7.25 ± 0.33
532	1479	1494	+7.44 ± 0.30
527	1523	1538	+8.70 ± 0.31
531	1566	1581	+8.36 ± 0.24
526	1610	1624	+6.78 ± 0.30

Table A.4 (continued)

Tape no.	v_{NO} [m/s]	$\langle v_{rel} \rangle$ [m/s]	A(exp) [°/oo]
530	1653	1667	+5.83 ± 0.26
533	1697	1711	+3.39 ± 0.33
550	1783	1796	-1.41 ± 0.32
547	1870	1884	-6.10 ± 0.31
548	1957	1970	-11.15 ± 0.36
549	2044	2057	-14.66 ± 0.47
556	2115	2128	-16.92 ± 0.78
558/559	2284	2297	-23.00 ± 0.48
560	2369	2382	-22.53 ± 0.81

Table A.5. NO-Xe

Tape no.	v_{NO} [m/s]	$\langle v_{rel} \rangle$ [m/s]	A(exp) [°/oo]
135	433	465	-6.25 ± 0.34
137	455	486	-6.05 ± 0.32
133	476	506	-6.00 ± 0.36
132	498	526	-5.89 ± 0.34
130/131	541	567	-5.53 ± 0.16
139	563	588	-5.07 ± 0.29
134	585	609	-5.17 ± 0.26
253/254	665	687	-2.82 ± 0.81
310	676	698	-2.98 ± 0.69
299	710	731	-4.22 ± 1.00
413	731	751	-6.25 ± 1.20
298/414/415	754	774	-6.37 ± 0.70
300/	777	797	-8.95 ± 0.56
266	787	806	-9.00 ± 0.94
301	811	830	-7.01 ± 0.53
302	845	863	-5.05 ± 0.66
339	879	896	-1.52 ± 0.74
337	913	930	+1.68 ± 1.02
367	947	964	+3.54 ± 0.65
334	990	1006	+3.57 ± 0.82
332	1014	1030	+4.60 ± 1.10
365	1047	1063	+3.90 ± 0.54

Table A.5 (continued)

Tape no.	v_{NO} [m/s]	$\langle v_{rel} \rangle$ [m/s]	A(exp) [°/oo]
333	1080	1095	-1.00 ± 0.88
334/342	1113	1128	-5.43 ± 0.39
343	1152	1167	-7.61 ± 0.50
368/395	1186	1200	-10.23 ± 0.99
396	1234	1248	-11.91 ± 1.20
397	1280	1294	-17.49 ± 1.15
536	1305	1329	-17.34 ± 0.30
410	1325	1338	-17.29 ± 1.00
411	1371	1384	-14.19 ± 0.85
538	1436	1449	-11.09 ± 0.30
539	1523	1536	-4.88 ± 0.28
540	1610	1622	+2.27 ± 0.27
541	1697	1709	+6.11 ± 0.35
542	1784	1796	+9.36 ± 0.41
543	1870	1882	+8.44 ± 0.28
544	1958	1969	+6.34 ± 0.35
545	2045	2056	+2.44 ± 0.36

B1. SERIES EXPANSION FOR THE MS POTENTIAL

Analogue to ref. 1, for the Maitland-Smith potential, coefficients of E^{*-n} are given for the reduced quantities $l_m^* = l_m/kR_e$, $\eta_m^* = \eta_m/kR_e$, $\eta_m^{*\prime\prime} = -d^2\eta_m^*/dl_m^2|_{l_m^*}$ (Table B.1) and the $S^{(m)}$-integrals (Table B.2). We used $E^* = F/\varepsilon$, where E stands for the centre of mass energy. One should notice that the coefficients for $S^{(m)}$ are a factor $2^{1/6}$ smaller as compared to the equivalent coefficients calculated according to ref. 2, due to the slightly different definition.

REFERENCES

1. R.B. Bernstein and R.A. LaBudde, J.Chem.Phys. 58 (1973) 1109

2. D. Klaassen, H. Thuis, S. Stolte and J. Reuss, Chem.Phys. 27 (1977) 107

Function	n = 0	1	2	3	4	5	6
η_m^*		0.39182	-0.09382	-0.1270	0.2435	-0.115	
l_m^*	0.95136	0.31288	-0.1291	0.0150	0.010		
$-\eta_m^{*\prime\prime}$		26.4486	-143.1	444.8	-755.1	637.7	-208.7

Table B.1. Expansion coefficients of terms in the $-n^{th}$ power of E^* for n = 0, ..., 6.

n	$S^{(m)}(a,0,0)$	$S^{(m)}(a,0,2)$	$S^{(m)}(r,0,0)$	$S^{(m)}(r,0,1)$	$S^{(m)}(r,0,2)$
0	0.6822193	0.5777855	0.2834347	0.2737942	0.2650137
1	-0.2029890	-0.1292738	0.0654698	0.0743662	0.0818027
2	-5.5500775	-4.1339656	-4.2256815	-4.0053361	-3.8084973
3	62.028622	45.347506	4.3988769	41.428842	39.158992
4	-367.83682	-269.25282	-259.54488	-244.54844	-231.24164
5	1291.0952	947.81780	912.86586	860.93763	814.78358
6	-2792.9524	-2054.8526	-1979.2295	-1867.9774	-1768.9394
7	3762.7148	2772.2058	2670.7913	252.18538	2389.0790
8	-3075.9467	-2268.0314	-2185.5428	-2064.2611	-1955.9989
9	1396.6640	1030.1967	992.91000	937.95940	888.84636
10	-270.27931	-199.37185	-192.18361	-181.55944	-172.05233

Table B.2. Expansion coefficients for the $S^{(m)}$-integrals of terms in $-n^{th}$ power of $E^{\star}$ for the MS potential with $\gamma = 10$.

C1. THE PROBING DISTANCE OF A_{ng}

We replace the V_2-term of the MS-potential by $\alpha.\delta(R-R')$ where α remains undetermined as the result is given in arbitrary units. The relative contribution of such an AIP to the nonglory anisotropy, A_{ng}, is found in lsa (ref. 1)

$$\Delta A_{ng} = (1/\bar{\sigma})\frac{3}{2}.4\pi\int bdb[-<\frac{1}{\hbar}\int_{-\infty}^{\infty} V'(t)dt>\sin 2\eta_{1,0}] ,$$

with

$$<\frac{1}{\hbar}\int_{-\infty}^{\infty} V'(t)dt>_{3/2} \xrightarrow{\delta\text{-function}} -\frac{4\pi}{5\hbar v_{rel}} \alpha <P_2(\hat{r}_1.\hat{z})>_{3/2} \times$$

$$[\frac{3}{2}\frac{(R')^2 - b^2}{(R')^2} - \frac{1}{2}]R'/((R')^2 - b^2)^{1/2} \quad \text{for} \quad R' \geq b$$

$$\xrightarrow{\delta\text{-function}} \quad \text{zero} \quad \text{for} \quad R' \leq b,$$

$$<P_2(\hat{r}_1.\hat{z})>_{m_j} = \frac{j(j+1) - 3m_j^2}{j(j+1)} \cdot \frac{j(j+1) - 3\Omega^2}{j(j+1)}$$

and

$$\bar{\sigma} = 4\pi\int bdb[1 - \cos 2\eta_{1,0}]$$

The expectation value $<...>_{m_j}$ has to be taken with the rotational state function characterized by j, Ω and m_j.

Numerical results are displayed in Fig. C.1.

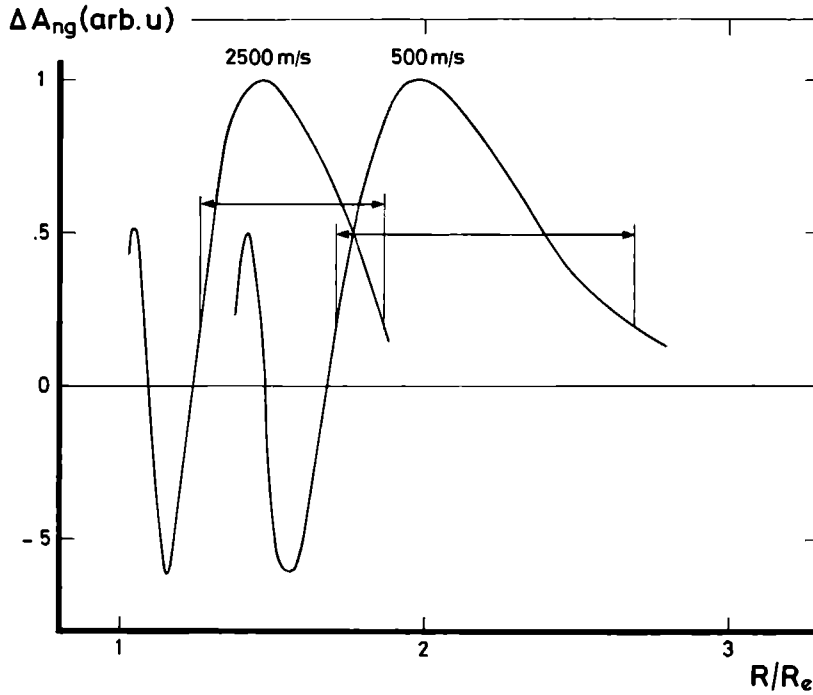

Fig. C.1. The sensitivity curve for the non glory contribution of the anisotropy, A_{ng}, vs. the reduced intermolecular distance R/R_e. The arrows indicate the range mainly probed, by one velocity setting. The probing distance is calculated for the high and low experimental velocity limits. At the left the beginning of a strongly oscillating behaviour - averaging to zero - is shown.

C2. THE PROBING DISTANCE OF A_g

For the glory part A_g one has in sa (ref. 1)

$$A_g = -\frac{1}{\sigma} l_{m,0} \left(\frac{\pi}{|\eta''_{m,0}|}\right)^{1/2} \{ \langle \cos [2\eta_{m,0} - \frac{\pi}{4} - \frac{1}{\hbar} \int_{-\infty}^{\infty} V'(t)dt] \rangle_{3/2} - \langle \ldots \rangle_{1/2} \}$$

where $\langle \ldots \rangle_{3/2(1/2)}$ stands for the expectation value taken with the $j = \Omega = 3/2$, $m_j = 3/2(1/2)$ rotational state function. The integral $\int_{-\infty}^{\infty} V'(t)dt$ is calculated using curved but undeflected trajectories leading to the S-integrals defined in ref. 1.

A_g is obtained by employing both $V' = V_2(R)P_2(\cos\vartheta)$ (yielding A_g) and V'' (yielding $\tilde{A}_g$). For $R' \leq R < R' + \Delta R$ one has $V'' = 0$ and $V'' = V_2(R)P_2(\cos\vartheta)$ elsewhere.

The difference $\Delta A_g = A_g - \tilde{A}_g$ is displayed, for $\Delta R = 0.02$ Å at $v_{rel} = 1900$ m/s. The result is rather independent of velocity but becomes less broad for smaller ΔR. For the MS potential ΔA_g is displayed in Fig. C.2.

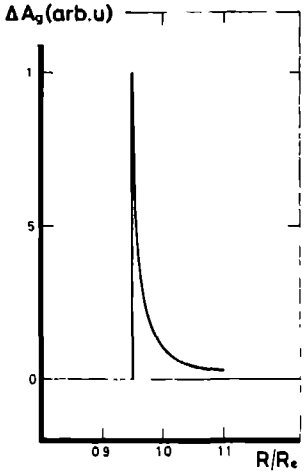

Fig. C.2. The sharply peaked sensitivity curve for the glory contribution of the anisotropy, ΔA_g, is rather independent of velocity and shows maximum at $R/R_e = 0.96$.

REFERENCE

1. S. Stolte and J. Reuss in Atom-molecule collision theory: A guide for the experimentalist, Ed. R.B. Bernstein, Plenum Press, New York, 1979

In dit proefschrift wordt een experimenteel onderzoek van de hoekafhankelijkheid van de intermoleculaire potentiaal op afstanden die in de buurt van het potentiaal-minimum liggen, beschreven. De gebruikte toestandsselectie van NO-moleculen is een essentiële voorwaarde om de totale botsingsdoorsnede voor twee verschillende oriëntaties te kunnen meten. De keuze van NO wordt bepaald door zijn bijzonder gunstige eigenschappen: lineair Stark-effect en groot Zeeman effect, massa spectrometrisch zonder moeilijkheden te detecteren en lage prijs. Hiernaast is NO een veel voorkomend en chemisch interessant molecuul met een niet gesloten electronenschil.

De anisotropie, het verschil tussen de totale botsingsdoorsnede voor twee onderling loodrechte voorkeursoriëntaties, is over een groot snelheidsgebied gemeten voor de systemen NO-Ne, -Ar, -Kr, en -Xe. Voor de theoretische beschrijving is uitgegaan van een intermoleculaire potentiaal van de vorm $V(R,\vartheta) = V_0(R) + V_1P_1(\cos\vartheta) + V_2(R)P_2(\cos\vartheta)$, waarbij R de intermoleculaire afstand is en P_n de n-de orde Legendre polynoom die afhangt van de hoek ϑ tussen de moleculaire as en de intermoleculaire plaatsvector.

Voor het systeem NO-Ar werd door de Leidse groep de totale botsingsdoorsnede zonder toestandsselectie gemeten. De gecombineerde data stelden ons in staat om verschillende potentiaal modellen te vergelijken en de parameters voor V_0, V_1 en V_2 vast te leggen voor het best fittende model, de Maitland-Smith potentiaal (hoofdstuk 4).

De berekeningen zijn gebaseerd op de "sudden approximation" waarbij ook rekening wordt gehouden met hogere orde effecten van de hoekafhan-

kelijke termen van de potentiaal. Andere beschikbare benaderingswijzen, zoals linear sudden (lsa), distorted wave (dwa) en infinite order sudden (IOS) blijken niet te voldoen.

Het is een veel voorkomend verschijnsel dat een potentiaal model dat een bepaald experiment beschrijft, ongeschikt is voor een ander. Daarom is in dit proefschrift ook aandacht besteed aan de vraag voor welk gebied van de potentiaal de beschreven experimenten gevoelig zijn.

De schrijver van dit proefschrift werd geboren op 20 januari 1947 te Huissen. Van 1959 tot 1963 bezocht hij de Titus Brandsma ULO en van 1963 tot 1966 het Thomas à Kempis College beide te Arnhem en legde in 1966 zijn eindexamen HBS-B met goed gevolg af. Vanaf januari 1967 tot september 1968 vervulde hij zijn militaire dienstplicht. In 1968 ging hij natuurkunde studeren aan de Katholieke Universiteit te Nijmegen en legde in maart 1971 zijn kandidaatsexamen af gevolgd door het doctoraal examen op 5 juli 1974. Tijdens zijn afstudeerperiode is hij werkzaam geweest in de werkgroep Vaste Stoffysica onder leiding van Prof.dr. P. Wyder. Na het behalen van zijn doctoraalexamen werd hij als wetenschappelijk medewerker in FOM-verband aangesteld in de werkgroep Atoom- en Molecuulfysica en verrichtte onder leiding van Prof.dr. J. Reuss en Dr. S. Stolte onderzoek aan de anisotrope potentiaal van NO-edelgassystemen, het onderwerp van dit proefschrift.

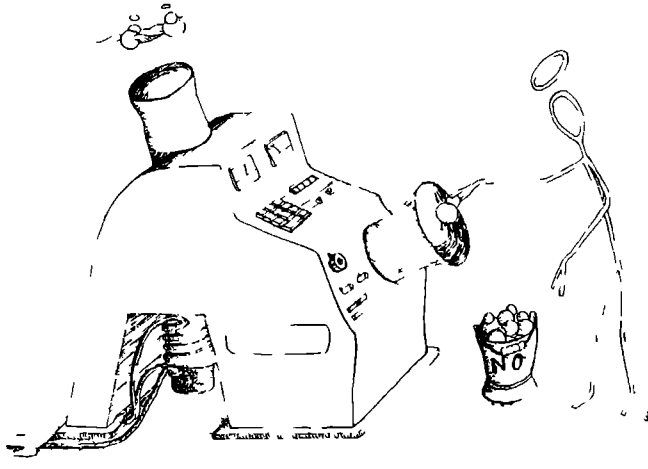
NO

STELLINGEN

1. Bij de calibratie van de absolute waarde van de chemiluminescente botsingsdoorsnede door Redpath et al. wordt geen rekening gehouden met de verschuiving naar het blauw van het geemitteerde spektrum bij toenemende botsingsenergie. De uitspraken dienen beperkt te blijven tot het "zichtbare" deel van het spektrum en leiden tot een botsingsdoorsnede die een faktor 10^3 kleiner is dan de voorspelde.

A.E. Redpath, M. Menzinger and T. Carrington
Chem.Phys. 27 (1978) 409

2. J. Verberne et al. hebben bij de bepaling van de rotatietemperatuur niet aan enkelvoudige lijnen gemeten, hetgeen tot aanzienlijke afwijkingen in de bezettingsgetallen kan leiden.

J. Verberne, I. Ozier,
L. Zandee and J. Reuss
Mol.Phys. 35 (1978) 1649

3. Hoewel M. Mizushima opmerkt vroegere publikaties betreffende de rotatie-energieën van een $^3\Sigma$-toestand te hebben gecorrigeerd, zijn de door hem gegeven uitdrukkingen nog steeds onjuist.

M. Mizushima
The theory of rotating diatomic molecules
John Wiley and Sons, New York (1975)

4. Bij metingen zoals beschreven in dit proefschrift moet men zich realiseren dat het gebied waar zij gevoelig zijn (harde botsingen, korte afstand kleiner dan het van der Waals minimum) zich bevindt op de uiterste staart van de elektronendichtheidsverdeling rond de kernen.

5. Bij bundelexperimenten waarbij het hoekoplossend vermogen een belangrijke rol speelt voor de interpretaties van de meetresultaten is het in een aantal gevallen mogelijk en aan te bevelen een methode analoog aan de wiebelende zespool te gebruiken.

Dit proefschrift

6. De metingen van N. Lee en J. Fenn aan dimeer-concentraties in argonbundels zijn op theoretisch onjuiste wijze geanalyseerd; ook moet de afhankelijkheid van de gemiddelde snelheid van de brondruk bij de analyse betrokken worden.

N. Lee and J. Fenn
VI International symposium on molecular beams (1977)

7. Hoewel de elegante time of flight methode in het algemeen "computer geschikte" data oplevert zodat men op eenvoudige wijze tot inzicht in de energie-afhankelijkheid van verschillende processen kan komen, zijn er een aantal experimenten waarbij het gebruik van een mechanisch veel storingsgevoeliger snelheidsselector zeer te preferen is.

8. De uitdrukking zoals afgeleid door D. Secrest voor de intermolekulaire wisselwerking transformeert niet als een scalar.

D. Secrest
Atom-molecule collision theory. A guide for the experimentalist
R.B. Bernstein (Ed.) Plenum Press, New York (1979)